NASA Contractor Report 3296

Selected Winglet and Mixed-Flow Long-Duct Nacelle Development for DC-10 Derivative Aircraft

Summary Report

A. B. Taylor

CONTRACT NAS1-14743
JUNE 1980

NASA

NASA Contractor Report 3296

Selected Winglet and Mixed-Flow Long-Duct Nacelle Development for DC-10 Derivative Aircraft

Summary Report

A. B. Taylor
McDonnell Douglas Corporation
Long Beach, California

Prepared for
Langley Research Center
under Contract NAS1-14743

National Aeronautics
and Space Administration

**Scientific and Technical
Information Office**

1980

FOREWORD

This document summarizes contract work performed for the NASA Energy Efficient Transport (EET) project of the Aircraft Energy Efficiency (ACEE) program by the Douglas Aircraft Company.

The NASA EET Project Manager was Mr. W. J. Alford of the Energy Efficient Transport Project Office at the Langley Research Center. His technical monitor was Mr. D. L. Maiden. The NASA on-site representative was Mr. J. R. Tulinius. The principal Douglas personnel responsible for this work were:

M. Klotzsche	ACEE Program Manager
A. B. Taylor	EET Project Manager
J. E. Donelsen	Aerodynamics Engineering
R. D. Gilkey	Aerodynamics Engineering
S. P. Patel	Aerodynamics Engineering
O. D. Wells	Aerodynamics Engineering

CONTENTS

ILLUSTRATIONS

ILLUSTRATIONS (Continued)

SUMMARY

The contract activity investigated the high-speed cruise drag effects of the installation of winglets and a wing-tip extension, and of a mixed-flow long-duct nacelle.

The winglet program utilized a 4.7-percent semispan model in the NASA Langley Research Center 8-foot transonic wind tunnel. Winglets were found to provide approximately twice as much cruise drag reduction as wing-tip extensions, for about the same increase in bending moment at the wing-fuselage juncture. Winglet drag improvements were in close agreement with analytical estimates.

The long-duct nacelle interference drag investigation utilized the same model, without the winglets, in the NASA Ames Research Center 11-foot transonic wind tunnel. The long-duct nacelle, installed in the same position as the current short-duct nacelle and with the current production symmetric pylon, was found to be a relatively low-risk installation. A pylon with an additional small rearward fairing was also tested and showed some drag reduction potential over the current pylon.

Technology recommendations for follow-on work concentrate on winglet development. High-lift aerodynamic wind tunnel development and flutter development are the major areas for near-term investigation, together with assessment of installation effects on aircraft performance. Some further high-speed wind tunnel exploration for the long-duct nacelle is also recommended for evaluation of nacelle shape changes.

INTRODUCTION

The research work effort summarized in this report has been performed as a part of the Aircraft Energy Efficiency (ACEE) program established within the NASA. The ACEE program was established to expedite industry application of advanced aerodynamic, active control, propulsion, and composite material technologies on fleet aircraft in order to improve both fuel efficiency and operational economics. Within this activity, the Energy Efficient Transport (EET) project has focused on advanced aerodynamics and active controls. The objective of the Douglas EET effort is to promote the near-term application of two aerodynamic concepts, winglets and mixed-flow long-duct nacelles (LDN). Fuel savings of as much as 11 percent could be achieved by the appropriate contributions of drag reduction and improvement in propulsive efficiency from these two concepts, although further study is needed to determine the net performance benefit considering all other aspects. It is believed that, with a favorable and energetic development program, the application of these concepts could be made for derivative aircraft scheduled for introduction in the early-to-mid 1980's time period.

DC-10 Winglet Investigation

Winglets are nonplanar, wing-tip mounted surfaces intended to provide greater drag reduction benefits at cruise than planar extensions imposing the same added bending moments on the wing structure. These surfaces, like wings, must be carefully designed to efficiently produce large normal forces inclined such that one component is directed forward. This component couples with the reduced induced drag of the wing to diffuse and weaken the tip vortex flow. The representation in Figure 1 shows a DC-10 equipped with winglets.

The purpose of the current investigation was to develop the cruise drag reduction potential of winglets and to evaluate these winglets relative to a wing-tip extension. The investigation was

FIGURE 1. DC-10 WITH WINGLETS

conducted in the Langley Research Center 8-foot transonic pressure wind tunnel (hereafter referred to as LRC 8-foot wind tunnel) in October and November 1977. It employed a 4.7-percent-scale semispan model of a DC-10 Series 10 (domestic version) and Series 30/40 (intercontinental version) wide-body transport. Winglets were evaluated on both the Series 10 and the Series 30/40 versions. A wing-tip extension, representing the change from the Series 10 to Series 30/40 configuration, was tested for comparison (Figure 2).

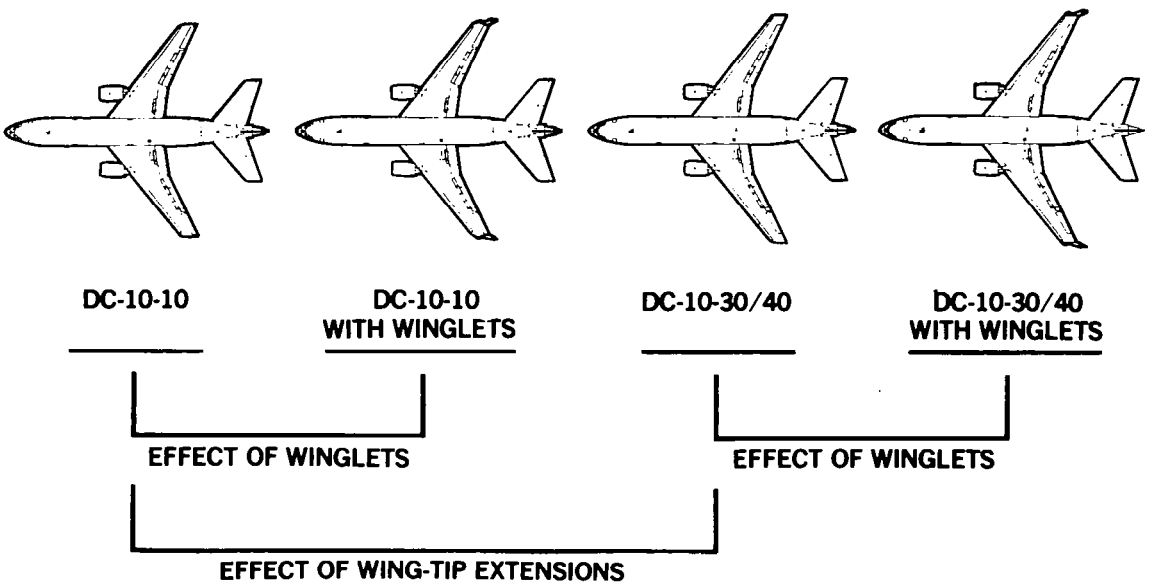

FIGURE 2. DC-10 AIRCRAFT CONFIGURATIONS FOR EVALUATION OF WINGLETS AND WING-TIP EXTENSION

Multiple winglet incidence angles were provided on each winglet. Development of the wing-to-winglet configuration was made to effect improvements in drag and observed flow characteristics. The effect of the addition of a lower winglet was also assessed.

The contract work is reported in detail in Reference 1.

Long-Duct Nacelle Investigation

For the DC-10, the LDN concept was first explored in an investigation of the application of lightweight composite materials and the potential reduction in community noise. Its potential for reduction in fuel consumption has now become attractive. The LDN carries the outer (fan) duct past the core nozzle, which incorporates a forced mixer. The gains arise from an improvement in propulsive efficiency due to the internal mixing of the fan and primary flow streams which, in the current production nacelle, exit separately at different velocities; advantages also result from the elimination of the nacelle afterbody fan exhaust scrubbing drag. Disadvantages are that the freestream scrubbing drag is increased due to the longer fan cowl and the nacelle weight is increased. A further possible improvement could result from a reduction in the wing-pylon-nacelle

channel velocities that result from the influence of the wing pressure flow field on the nacelle cyclic flow field. It was estimated that a net total reduction of four to five percent in fuel burned could be realized by the application of this concept. Figure 3 shows a DC-10 equipped with the LDN.

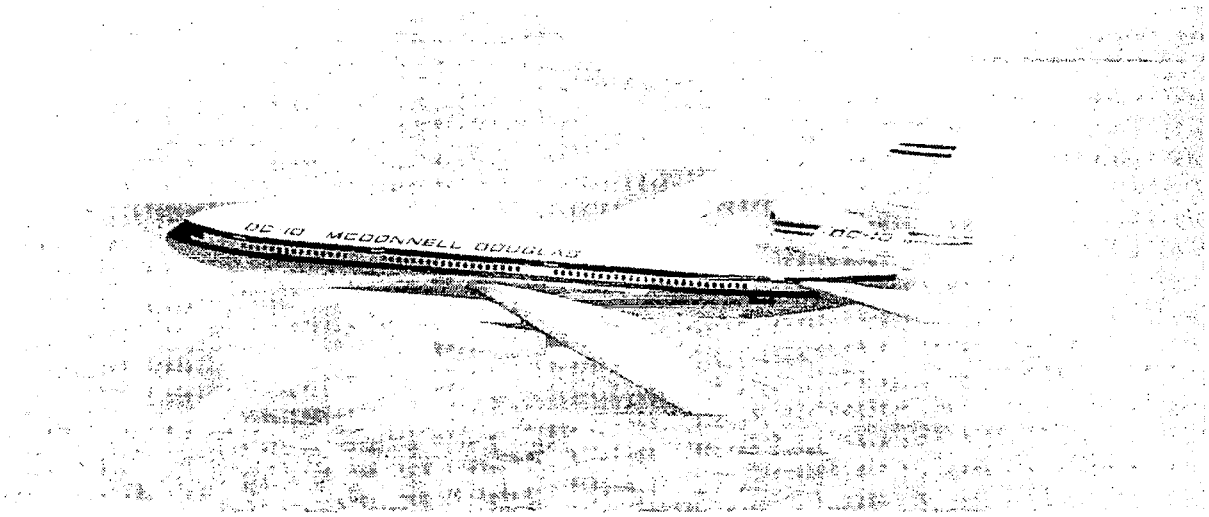

FIGURE 3. DC-10 WITH LONG-DUCT NACELLES

The program concerned itself with the task of integrating the nacelle, pylon, and wing at cruise speeds to achieve an installation with low interference drag, so that the potential gain is not diluted.

A method appropriate for application with minimum impact to a derivative of an existing aircraft is to camber the pylon streamwise sections on the inboard side. This method was the basis of the contract task.

The work was accomplished by a development program conducted in the Ames Research Center 11-foot transonic wind tunnel (hereafter referred to as the ARC 11-foot wind tunnel) in June and July 1978. The program had two parts: an isolated nacelle and pylon calibration test, and a semispan model test. The model scale was 4.7 percent, the nacelles and wing configuration representing a DC-10 Series 30. The baseline nacelle was the current production type, a short-duct nacelle (SDN). The side profiles of the two nacelles are shown in Figure 4.

Baseline data and power effects for the LDN were measured using a turbosimulator, representing the General Electric CF6-50 engine which powers the DC-10 Series 30. The DC-10 Series 40, previously mentioned in the introduction to the winglet task, is powered by Pratt & Whitney engines. Although the Series 40 nacelles differ slightly in shape and size from those of the Series 30, it is considered that the conditions and results of the current study are applicable to them also.

CF6-50 MIXED-FLOW LDN

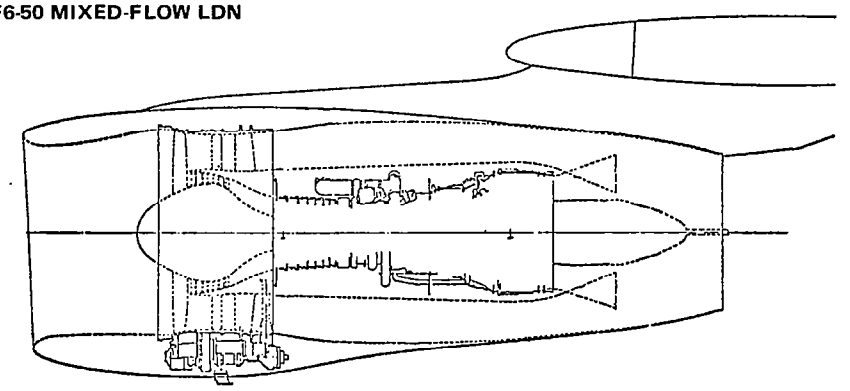

CF6-50 PRODUCTION SDN

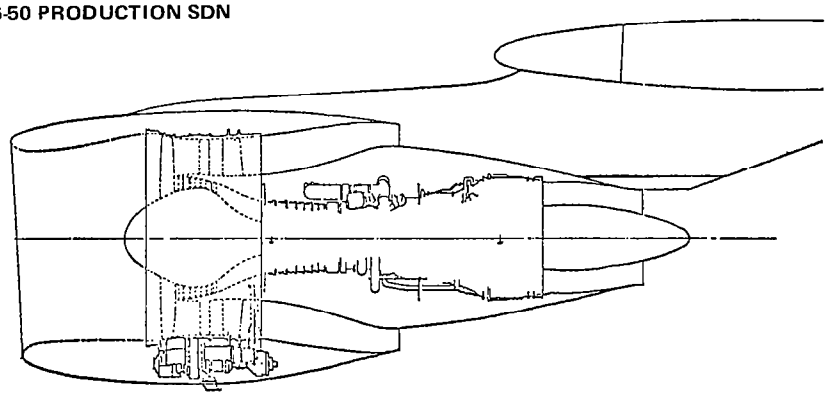

FIGURE 4. PROFILES OF SHORT- AND LONG-DUCT NACELLES

All the pylon designs tested had the LDN located in the same position relative to the wing as the SDN. The current pylon, having symmetrical streamwise sections, was used as the baseline. The effects of variation of nacelle incidence and of engine power were evaluated using the pylon. Two alternative pylons, one having a small aft fairing and another a large one, were designed to reduce local velocities in the inboard wing-pylon-nacelle channel, and these were evaluated using the flow-through nacelle.

The contract work is reported in detail in Reference 2.

Use of tradenames or names of manufacturers in this report does not constitute an official endorsement of such products or manufacturers, either expressed or implied, by the National Aeronautics and Space Administration.

Symbols and Nomenclature

Values are given in SI Units and also in U.S. Customary Units. Measurements and calculations were made in U.S. Customary Units.

ACEE	Aircraft Energy Efficiency (program)
ARC	Ames Research Center
b_A	semispan of DC-10 Series 10 wing model
b_B	semispan of DC-10 Series 30/40 wing model
C_D	drag coefficient, $Drag/q_\infty S$
ΔC_D	incremental drag coefficient
C_L	lift coefficient, $Lift/q_\infty S$
C_n	normal force
C_p	pressure coefficient, $\frac{p_\ell - p_\infty}{q_\infty}$
c	local chord, used nondimensionally
$\bar{c}_a$	mean aerodynamic chord of the DC-10 Series 10 wing model, 35.90 cm (14.13 in.)
$\bar{c}_b$	mean aerodynamic chord of the DC-10 Series 30/40 wing model, 35.31 cm (13.9 in.)
c_ℓ	section lift-force coefficient
c_y	section side-force coefficient
EET	Energy Efficient Transport (program)
FWD	forward
h	winglet vertical height above wing tip, used for reference
INT	interference
LDN	long-duct nacelle
LRC	Langley Research Center
M_∞	free-stream Mach number
p_ℓ	local static pressure
p_∞	free-stream static pressure
q_∞	free-stream dynamic pressure
S	trapezoidal area of DC-10 Series 10 wing model, 0.7285 m^2 (7.8420 ft^2)
	trapezoidal area of DC-10 Series 30/40 wing model, 0.7485 m^2 (8.0574 ft^2)
SDN	short-duct nacelle
T.E.	trailing edge
x	chordwise distance aft of leading edge
α	angle of incidence
$\eta_{winglet}$	percent of winglet semispan measured from h = 0 reference

Configuration Design

The DC-10 winglet, based on the design by Dr. R. T. Whitcomb of NASA Langley, utilizes the general guidelines published in Reference 3. Prior to selection of wind tunnel test configurations, evaluations were made of perturbations in winglet height, taper ratio, location, upper-lower combinations, and size. No significant improvements to the Whitcomb design were suggested. Test configurations used a NASA Langley modified GAW 8-percent-thick airfoil section and were untwisted.

Three configurations having upper and lower winglet surfaces were designed for the test program. Winglet A was utilized on the Series 10 wing and Winglet B on the Series 30/40 wing. Winglet C, also applied to the Series 30/40 wing, combined the upper portion of Winglet A with the lower portion of Winglet B.

As will be described, some details of the winglet geometry were modified during the winglet development phase of the test program. The geometry of the two wings and of the winglet systems as designed is shown in Figure 5 and Figure 6, respectively.

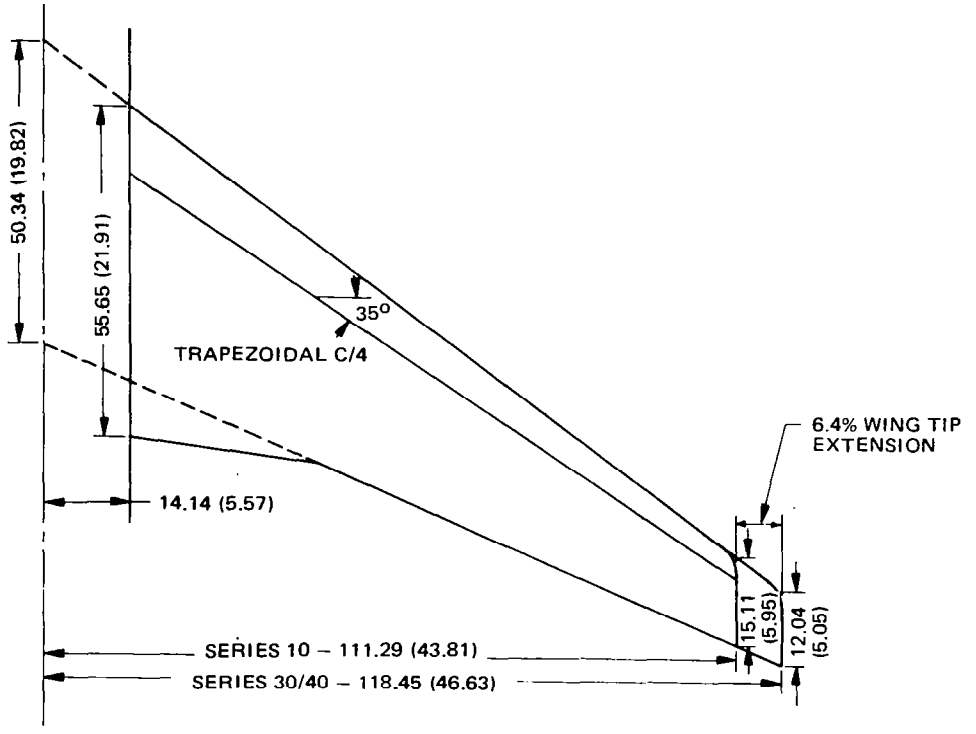

DIMENSIONS ARE IN CENTIMETERS (INCHES)

FIGURE 5. DC-10 MODEL WING GEOMETRY

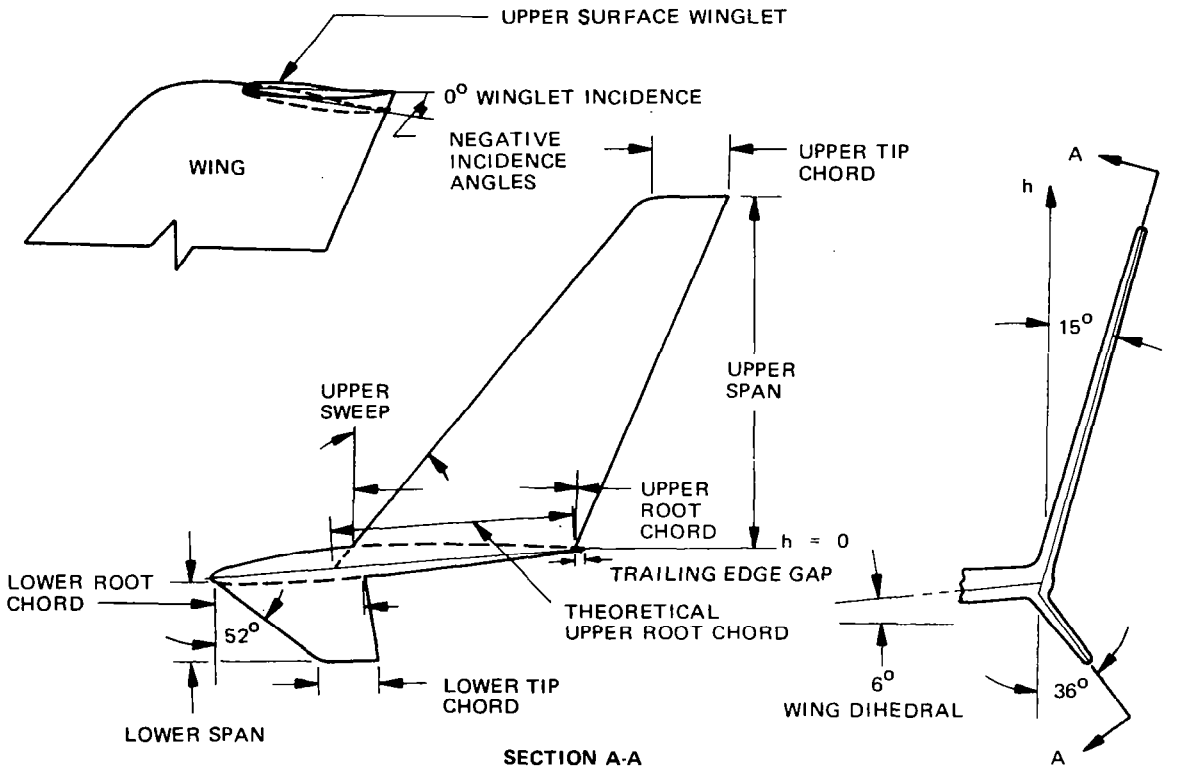

WINGLET CONFIGURATION	A	B	C
UPPER WINGLET			
SPAN	15.14 (5.96)	15.14 (5.96)	
ROOT CHORD	9.07 (3.57)	7.70 (3.03)	
TIP CHORD	2.72 (1.07)	2.29 (0.90)	AS A
SWEEP	40°	39°	
TRAILING EDGE GAP	0.51 (0.20)	0.51 (0.20)	
THEORETICAL ROOT CHORD (PROPORTION OF WING TIP CHORD)	0.65	0.65	0.77
LOWER WINGLET			
SPAN	3.34 (1.32)	3.33 (1.31)	
ROOT CHORD	6.06 (2.39)	5.13 (2.02)	AS B
TIP CHORD	2.53 (1.00)	1.46 (0.573)	

DIMENSIONS ARE IN CENTIMETERS (INCHES)

FIGURE 6. WINGLET MODEL DESIGN GEOMETRY

Experimental Apparatus and Procedures

The investigation was conducted in the LRC 8-foot wind tunnel. The 4.7-percent-scale DC-10 semispan model was mounted in an inverted position on the Langley 804-S balance on the side wall of the tunnel. The model was tested with tail surfaces removed and a flow-through nacelle and pylon mounted on the wing.

Capability was provided to test upper and lower winglets together and with the lower surface winglet removed. The upper winglets could be set to winglet root airfoil incidence angles relative to the fuselage centerline of 0, -2, or -4 degrees, where negative incidence angle is trailing edge inboard (i.e., in the direction to unload the upper surface winglet). The lower surface winglets were set at an incidence angle of zero degrees.

All testing was accomplished with boundary layer transition fixed.

The model was equipped for measuring force, moment, and pressure data. Oil flow visualization was used to determine flow quality in the area of the wing-winglet. The major portion of the measurements was taken over a Mach number range of 0.60 to 0.82 with the angle of attack of the model varied over a range corresponding to lift coefficient values between 0.40 and 0.60. A constant Reynolds number of 14.8 x 10^6 per meter (4.5 x 10^6 per foot) or 5.3 x 10^6 based on the mean aerodynamic chord of the DC-10 Series 10 was maintained. The Reynolds number was held to within ±32,800 per meter (±10,000 per foot) and the Mach number to within ±0.002 of the intended values throughout the test. The drag coefficient repeatability was generally within ±0.0002, while lift coefficient repeated within ±0.002.

Results and Discussion

The effects of the installation of winglets and wing-tip extension on the cruise drag are presented in the form of incremental drag coefficients, which include trim effects. No significant differences in pitching moment were noted between winglets and wing-tip extension configurations. These trim effects are typically one to one-and-one-half drag counts penalty at cruise lift coefficients. Lift data were acquired primarily for correlating drag at given values of lift.

Winglet Development on DC-10 Series 10 (Winglet A) — The upper surface winglet was tested at Mach numbers of 0.60, 0.74, and 0.82. A deterioration of the improvement was indicated with increasing Mach number. Fluorescent oil flow visualization indicated high cross flow and a separated region on the outboard surface of the lower winglet at the upper trailing edge for 0.74 and 0.82 Mach numbers, but not at 0.60 Mach number. The oil flow with the upper winglet alone indicated up-flow on the aft inboard surface of the upper winglet/wing juncture, increasing significantly with increasing Mach number.

The force data at 0.6 Mach number were used as a basis for conclusions on the potential of each configuration. Both the upper-and-lower and upper-alone configurations exhibited their best drag reduction at an incidence angle of -2 degrees. The upper-and-lower winglet configuration

offered considerably more drag reduction potential. The upper-and-lower winglet configuration at an upper incidence angle of -2 degrees was therefore selected for further development work to eliminate the flow separation at the higher Mach numbers.

The observed flow separation was eliminated by relocating the lower winglet forward to remove the overlap of the upper winglet leading edge and lower winglet trailing edge. The revised configuration A1, which included a small juncture fillet, is shown in Figure 7.

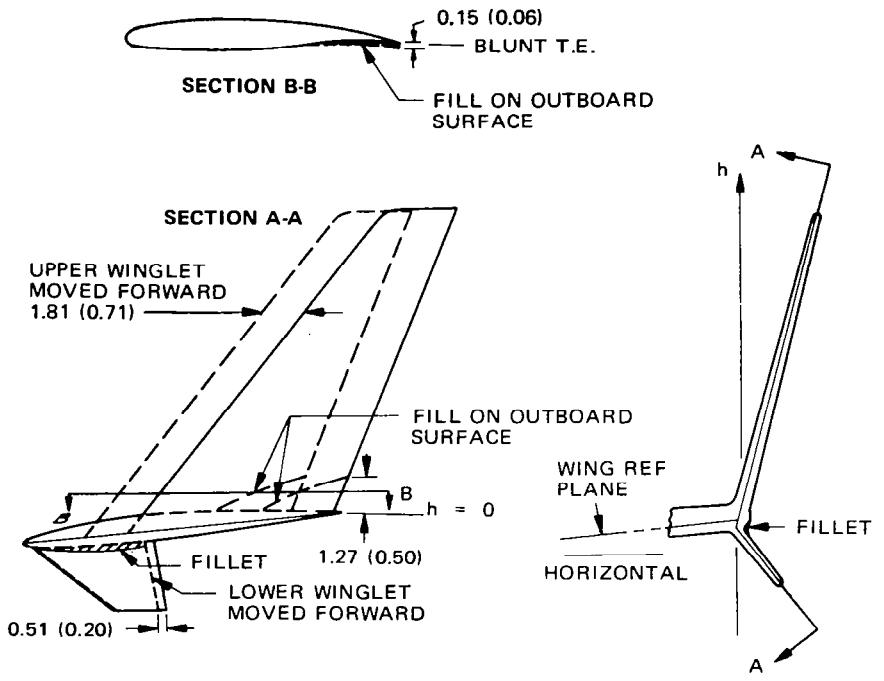

WINGLET A1 – WINGLET A AND LOWER WINGLET MOVED FWD 0.51 cm (L.E. CUT BACK AND RE-CONTOURED INTO WING-TIP L.E.) AND LOWER WINGLET FILL
WINGLET A2 – WINGLET A1 AND FILL ON UPPER WINGLET OUTBOARD SURFACE
WINGLET A3 – WINGLET A1 AND UPPER SURFACE WINGLET MOVED FWD
DIMENSIONS ARE IN CENTIMETERS (INCHES)

FIGURE 7. GEOMETRY OF WINGLET A DEVELOPMENT CONFIGURATION

Figure 7 also shows two additional modifications investigated in the test. Modification A2 consisted of a small triangular-shaped buildup of the outboard surface of the upper winglet near the trailing edge intersection with the wing-tip. The purpose of this modification was to improve the boundary layer in the wing-winglet intersection, but no change in drag improvement from A1 was exhibited. Winglet A2 was used for final data measurement.

Parametric studies had suggested a slight improvement of induced drag by moving the upper winglet forward, short of the position introducing wing and winglet peak velocity interference. In configuration A3, the upper winglet was moved forward. A significant performance loss at 0.74 and 0.82 Mach numbers was found, indicating that the aft position was the better.

Chordwise pressure distributions on the upper winglet of A2 (Figure 8) showed no indication of any flow problems on the winglet.

Spanload distributions are presented in Figure 9 for the wing alone and for the wing with winglet. As expected, the increased loading effect due to the addition of winglets is locally concentrated in the region of the wing-tip.

Winglet Development on DC-10 Series 30/40 (Winglets B and C) — The configuration modifications developed on Winglet A were incorporated into Winglet B (Figure 10). The upper surface winglet was tested at 0 and −2 degree incidence angles. At the cruise Mach number of 0.82, the -2 degree incidence position was slightly better, with no indication of flow separation problems.

A comparison of incremental drag results shows that Winglet C is superior to Winglet B (Figure 11). The figure also shows the drag reduction of the aircraft with Winglet C relative to the basic aircraft. No flow separation on Winglet C was indicated by oil flow pictures. Apparently, upper and lower surface interference is not significant for this case with a relatively larger upper and lower surface winglet overlap.

Chordwise pressure distributions on upper surface Winglet C (Figure 12) show no indications of any flow problem.

Span load distributions are presented in Figure 13 for the wing alone and for the wing with Winglet C installed. These show the expected effects due to the additon of the winglet.

Comparison of Estimated and Experimental Incremental Drag for Winglets and Wing-Tip Extensions — Figure 14 presents an incremental drag summary of the best Series 10 and Series 30/40 winglet and wing-tip extension wind tunnel results. These are compared with analytical

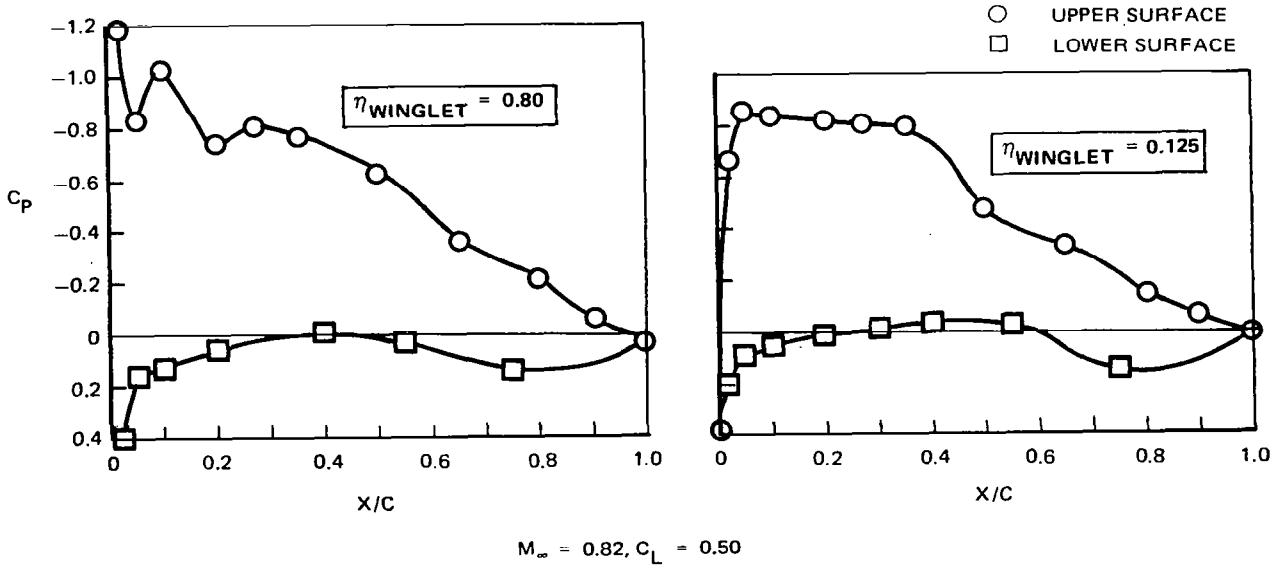

FIGURE 8. UPPER SURFACE WINGLET A2 CHORDWISE PRESSURE DISTRIBUTIONS

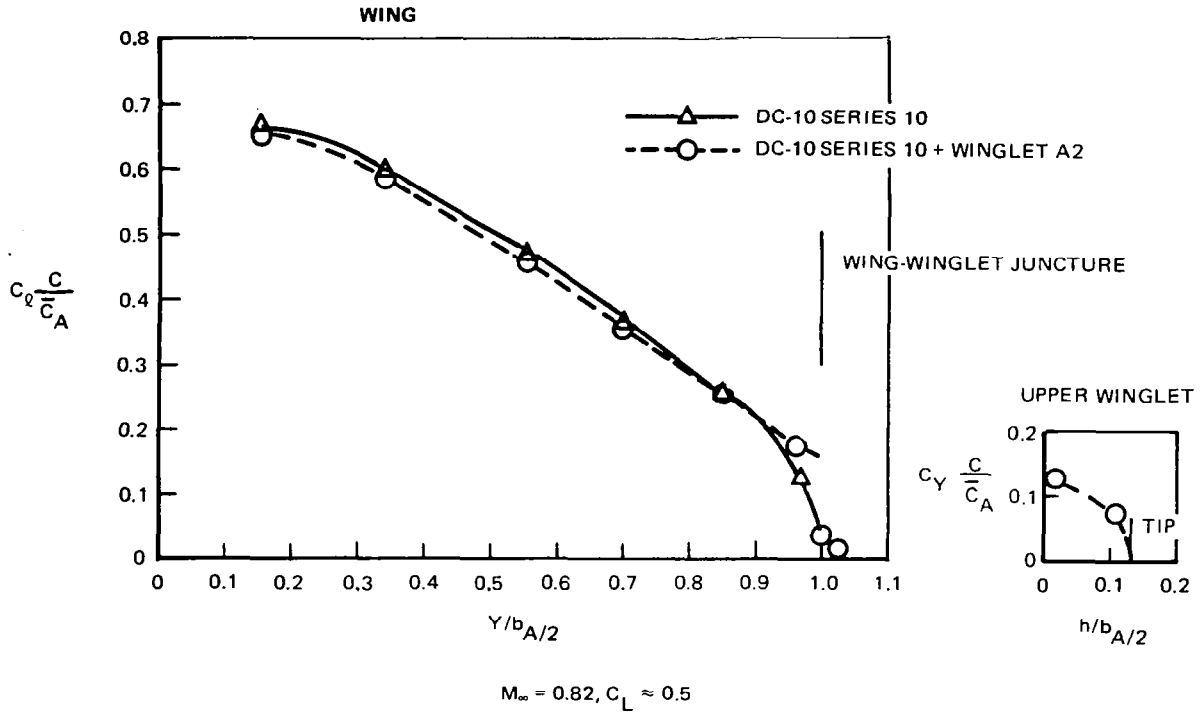

FIGURE 9. SPANWISE LOAD DISTRIBUTIONS FOR DC-10 SERIES 10 WITH AND WITHOUT WINGLET A2

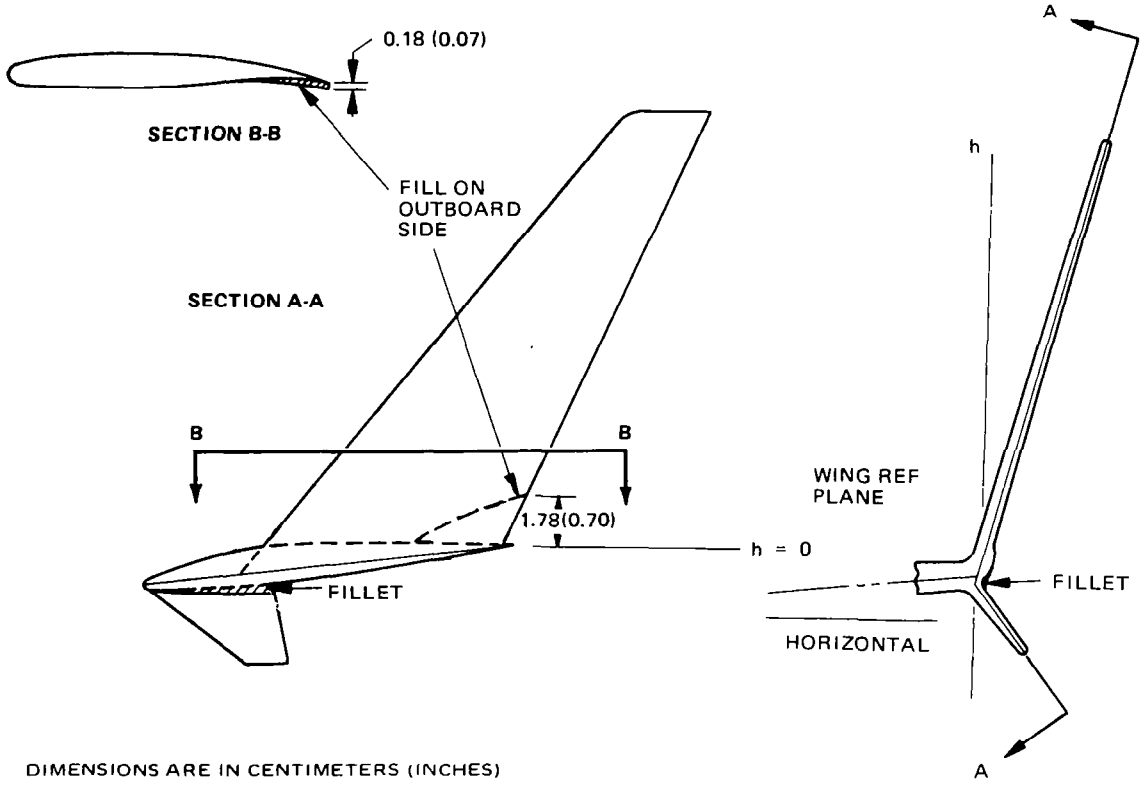

FIGURE 10. GEOMETRY OF WINGLET B TEST CONFIGURATION

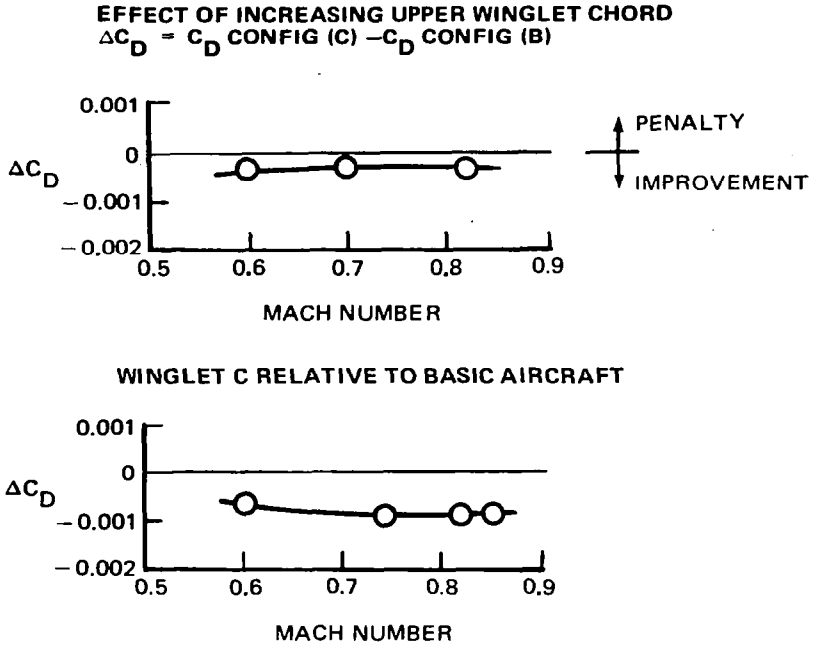

FIGURE 11. PERFORMANCE OF WINGLET C

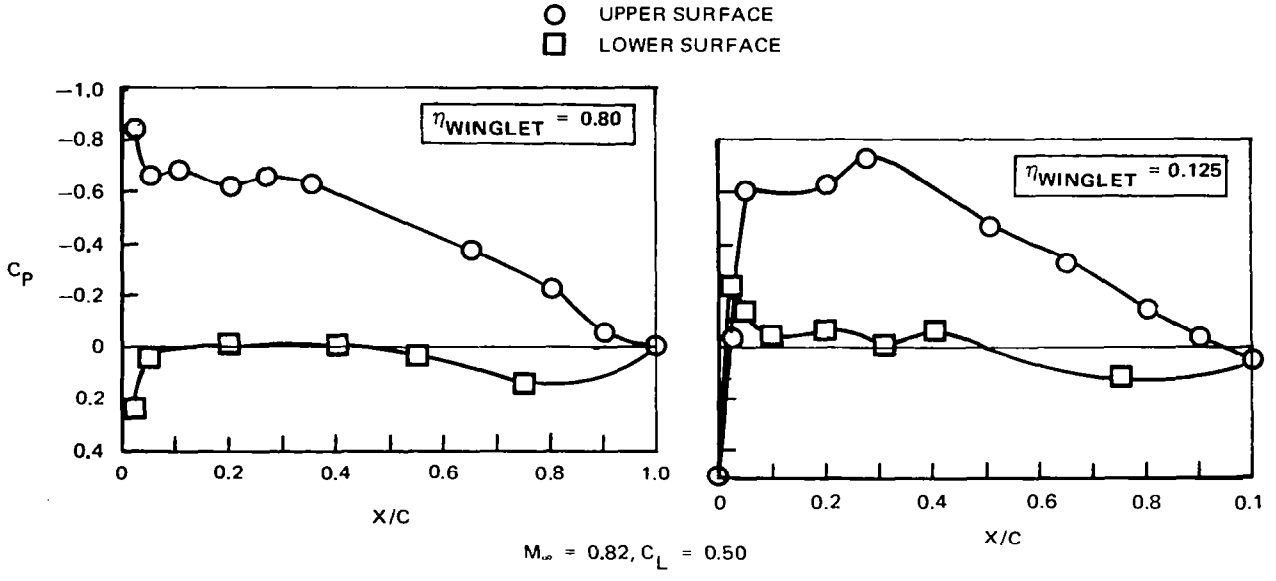

FIGURE 12. UPPER SURFACE WINGLET C CHORDWISE PRESSURE DISTRIBUTIONS

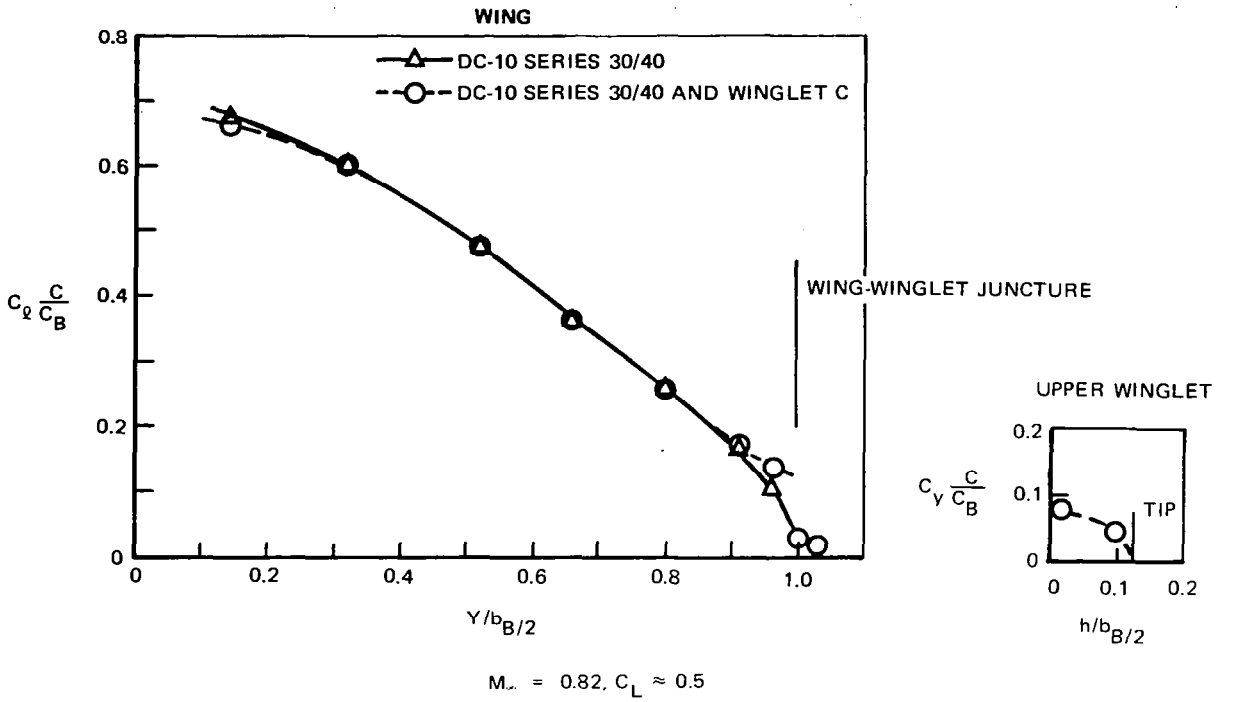

FIGURE 13. SPANWISE LOAD DISTRIBUTIONS FOR DC-10 SERIES 30/40 WITH AND WITHOUT WINGLET C

estimates of the induced drag improvements for a wing span loading corresponding to an 0.82 Mach number condition.

It has been found (Reference 3) that the largest measured reductions of drag due to adding the winglet are obtained with normal loads on the winglet less than suggested as optimum by the theory. As loading on the winglet increases, viscous drag effects increase and can offset improvements in wing-winglet induced drag.

Two levels of winglet performance estimates are shown in Figure 14. The optimum level was predicted to occur with an upper winglet incidence angle of zero degrees. However, the best performance results of the test were obtained with the winglet incidence off-loaded by two degrees (−2 degree incidence angle). The analytical prediction for the best winglet test configuration (−2 degree incidence) is included in the figure. It may may be seen that the best winglets for both the Series 10 and Series 30/40 achieved drag reductions somewhat less than the full analytical potential. However, the test data agree relatively well with the estimates at the same incidence angle.

Incremental Cruise Drag Data Summary — A summary of drag increments is presented in Figure 15, first for wind tunnel results and then after adjustment to flight Reynolds number. The data are for a range of Mach numbers and the most representative cruise lift coefficient. The Series 10 aircraft flies at an average cruise lift coefficient of approximately 0.45 and the heavier Series 30/40 at about 0.50. Data from the wind tunnel at a Reynolds number of 5.3×10^6 were ad-

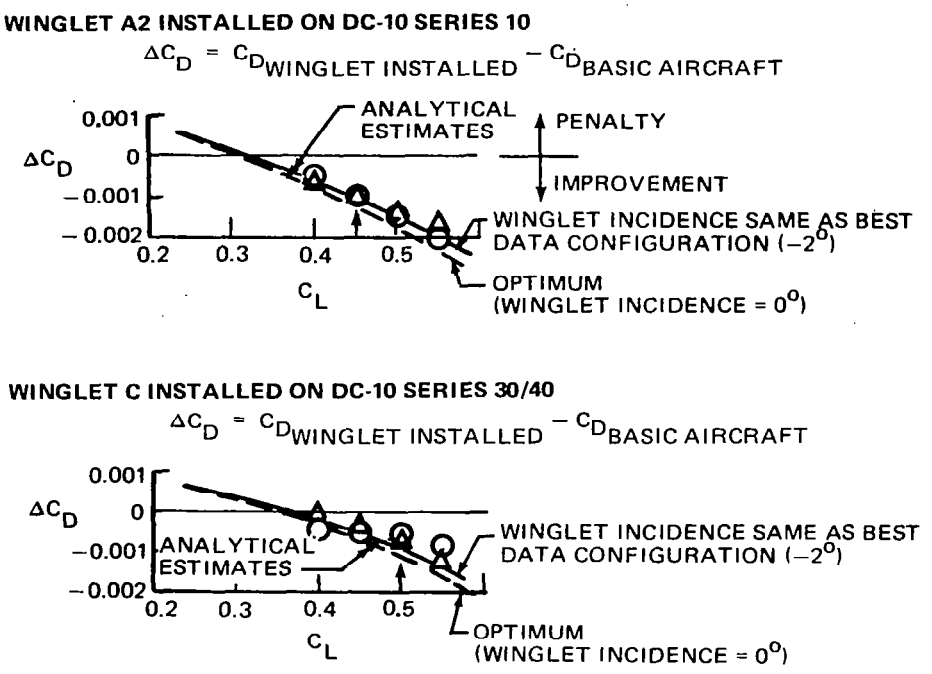

FIGURE 14. EFFECT OF BEST WINGLET AND WING-TIP ON INCREMENTAL CRUISE DRAG

justed to account for the flight Reynolds number of 5.0×10^7 (both numbers based on MAC). For the cruise conditions the incremental drag coefficient improvements for the installation of a winglet on the Series 10 and Series 30/40 are 0.0012 and 0.0010, respectively. The cruise condition incremental drag coefficient improvement for the wing-tip extension is 0.0009.

Winglets and Wing-Tip Extension Incremental Drag and Root Bending Moment Comparison – The comparative measured increase in wing root bending moment for winglets is compared to wing-tip extensions in Figure 16 for a fixed-lift coefficient of 0.5. The measured drag increments are corrected to flight Reynolds number. Regional shading of winglet performance compared

WIND TUNNEL REYNOLDS NUMBER

M	DC-10 SERIES 10 WINGLET A2 CRUISE C_L = 0.45 ΔC_D	DC-10 SERIES 10 + 6.4% WING-TIP EXT CRUISE C_L = 0.45 ΔC_D	DC-10-30/40 WINGLET C CRUISE C_L = 0.50 ΔC_D
0.60	0.00099	0.00062	0.00067
0.68	N/A	0.00058	N/A
0.74	0.00092	0.00064	0.00091
0.80	0.00096	0.00056	N/A
0.82	0.00100	0.00081	0.00085
0.85	0.00092	0.00077	0.00086

ADJUSTED TO FLIGHT REYNOLDS NUMBER

M	ΔC_D	ΔC_D	ΔC_D
0.60	0.00119	0.00071	0.00086
0.68	N/A	0.00067	N/A
0.74	0.00112	0.00073	0.00110
0.80	0.00116	0.00065	N/A
0.82	0.00120	0.00090	0.00104
0.85	0.00112	0.00086	0.00105

FIGURE 15. INCREMENTAL CRUISE DRAG DATA SUMMARY

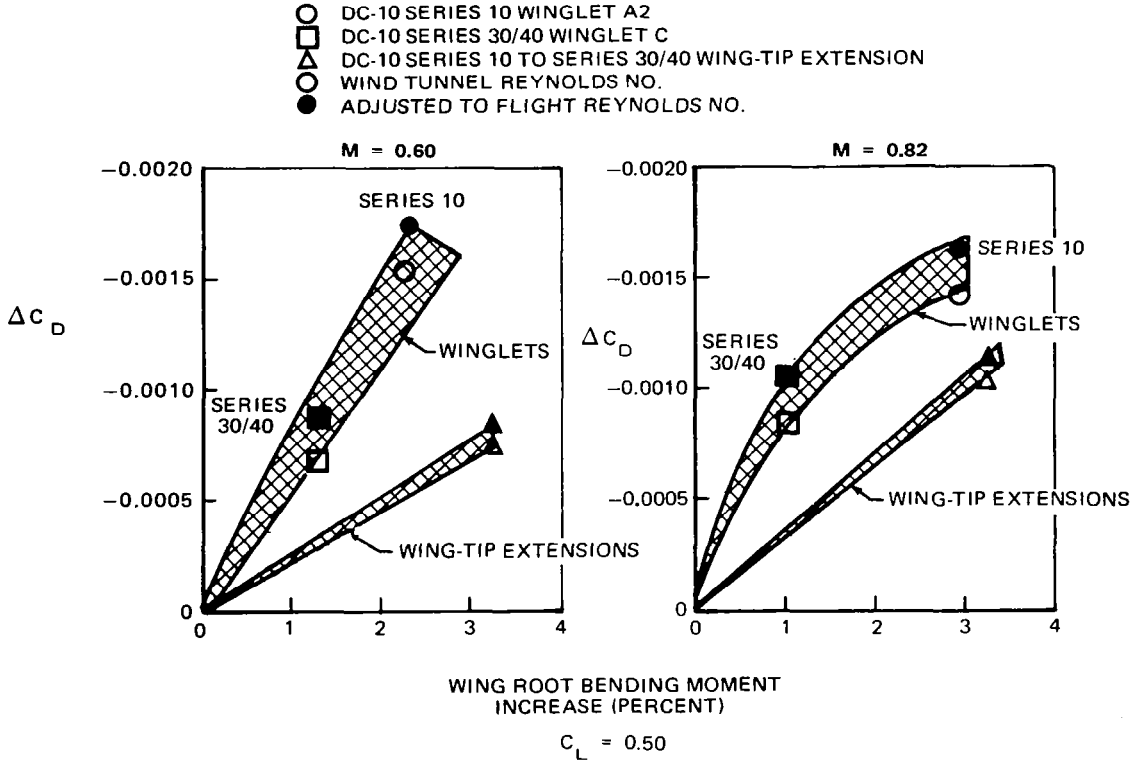

FIGURE 16. EFFECT OF WINGLETS AND WING-TIP EXTENSION ON INCREMENTAL CRUISE DRAG AND WING ROOT BENDING MOMENT

with wing-tip extension performance is shown. The increase in wing-root bending moment due to a wing-tip device is indicative of the resulting basic wing structural weight penalty. For a fixed value of drag improvement, winglets produce about one-half of the increase in wing-root bending moment as wing-tip extensions. Alternatively, for the same increase in wing-root bending moment, winglets provide approximately twice the drag improvements as wing-tip extensions.

INVESTIGATION OF THE INTERFERENCE EFFECTS OF MIXED-FLOW LONG-DUCT NACELLES ON A DC-10 WING

Nacelle-Pylon Configuration Design

Long-Duct Nacelle Design — The model nacelle was designed according to the recommendations reported in Reference 4, except that the inlet was modified to allow the proper simulation of inlet mass flow ratio and to preclude excess spillage drag. The current production DC-10 symmetrical pylon was selected as the baseline configuration, resulting in the retention of the SDN incidence of 0.9 degree nose up. Incidence angle variations of ±1.5 degrees from the baseline were incorporated into the pylon geometry in order to evaluate the minimum-drag incidence angle for the LDN. The current nacelle toe-in angle of 2.0 degrees was retained.

Pylon Fairing Design — A simplified potential flow panel model of the wing plus LDN and pylon was developed and used to evaluate a number of pylon configurations with systematic variations in shape. The study examined the effects of pylon leading and trailing edge camber and selected pylon fairings on the wing-pylon-nacelle channel pressure distributions. Selected configurations were subsequently evaluated with a more comprehensive fine panel model.

The pylon modifications considered during the design selection process and a summary of the results of the analysis are shown in Figure 17. The biggest benefit was predicted for Configurations E and G. Configuration E employed a small aft fairing, and Configuration G combined this fairing with an enlarged leading edge. These configurations were then investigated using the more detailed method. The previous estimates for Configuration G were found to be optimistic, and the more detailed was therefore discarded. Revisions to Configuration E were required to sustain its performance, and the resulting shape was denoted as Configuration J. In order to effect a further reduction in the channel peak pressures, a modification to the J fairing incorporating a larger aft fairing was defined (Configuration K). Configurations J and K were selected for the experimental work.

In each case, the pylon fairing was designed to be external to the DC-10 pylon, so that primary structure or systems routing would be unaffected.

The calculated potential flow pressure distributions on the wing lower surface, pylon, and nacelle in the vicinity of the inboard channel for the baseline symmetrical pylon, the small (Configuration J), and the large (Configuration K) pylon fairings are shown in Figure 18. The fairings reduce the levels of the suction peaks near the channel throat and increase the suction levels aft of the throat. These changes simultaneously tend to reduce the throat Mach number and the severity of the diffusion pressure gradient aft of the throat, and therefore reduce the tendency to shock drag and premature flow separation.

USING SIMPLIFIED NEUMANN PANEL GRID				
CONFIGURATION	TYPE OF FAIRING	REDUCTION IN WING LOWER SURFACE $C_{P_{PEAK}}$	WING LOWER SURFACE AND PYLON PRESSURE GRADIENT AFT OF $C_{P_{PEAK}}$	REMARK
	SYMMETRICAL		BASE	SYMMETRICAL PYLON IS USED AS THE BASELINE CONFIGURATION
A	SMALL AFT CAMBER	+0.01	WORSE	GRADIENT AFT OF PEAK PRESSURE IS MORE SEVERE ON WING LOWER SURFACE AND PYLON
B	LARGE AFT CAMBER	+0.04	WORSE	GRADIENT ON WING LOWER SURFACE AND PYLON IS MORE SEVERE AND WORSE THAN THAT WITH CONFIGURATION A
C	SMALL LEADING EDGE CAMBER	+0.02	SAME	NO CHANGE IN ADVERSE PRESSURE GRADIENT ON WING LOWER SURFACE AND PYLON
D	LARGE LEADING EDGE CAMBER	+0.06	SAME	NO CHANGE IN ADVERSE PRESSURE GRADIENT ON WING LOWER SURFACE AND PYLON
E	SMALL AFT FAIRING	+0.06	BETTER	LARGE REDUCTION IN PEAK PRESSURES AND ADVERSE PRESSURE GRADIENT ON WING LOWER SURFACE AND PYLON
F	LARGE LEADING EDGE FAIRING	+0.09	BETTER	LARGE REDUCTION IN PEAK PRESSURES AND LITTLE REDUCTION IN ADVERSE PRESSURE GRADIENT ON WING LOWER SURFACE AND PYLON
G	LARGE LEADING EDGE AND SMALL AFT FAIRING E + F CONFIGURATION	+0.10	BETTER	LARGE REDUCTION IN SUCTION PEAK PRESSURES AND ADVERSE PRESSURE GRADIENT REDUCTION IN PEAK PRESSURES FOR CONFIGURATIONS E AND F ARE NOT ADDITIVE

USING FINE NEUMANN PANEL GRID (SELECTED FOR AMES TEST)						
CONFIGURATION	TYPE OF FAIRING	REDUCTION IN $C_{P_{PEAK}}$			PRESSURE GRADIENT AFT OF $C_{P_{PEAK}}$ WING, PYLON, AND NACELLE	REMARK
		WING	PYLON	NACELLE		
J	SMALL AFT FAIRING SIMILAR TO 'E'	+0.07	+0.12	+0.08	BETTER	LARGE REDUCTION IN PEAK PRESSURES AND ADVERSE PRESSURE GRADIENT ON WING, PYLON, AND NACELLE
K	LARGE AFT FAIRING LARGER THAN 'J'	+0.10	+0.14	+0.15	MUCH BETTER	SUBSTANTIAL REDUCTION IN PEAK PRESSURES AND ADVERSE PRESSURE GRADIENT ON WING, PYLON, AND NACELLE

FIGURE 17. PYLON DESIGN ANALYSIS

Experimental Apparatus and Procedures

The test was conducted in the ARC 11-foot wind tunnel, using an isolated nacelle calibration model and a DC-10 semispan model. Both models were 4.7-percent scale and were mounted on the Langley 804S-B balance. All the models' components were provided with boundary layer transition strips.

The isolated nacelle and baseline pylon were mounted on a metric strut which was itself attached to the balance (Figure 19).

The semispan model was representative of the right half of the DC-10-30 aircraft except that the tail surfaces were removed. On this model, the turbosimulator SDN and LDN were tested with the baseline pylon. The flow-through LDN was tested with the baseline pylon and pylon fairing modifications. The semispan model installation is shown in Figure 20.

The powered SDN was representative of the DC-10 production nacelle for the General Electric CF6-50 engine. The TC-460 air-driven turbosimulator was used in the nacelle to simulate the

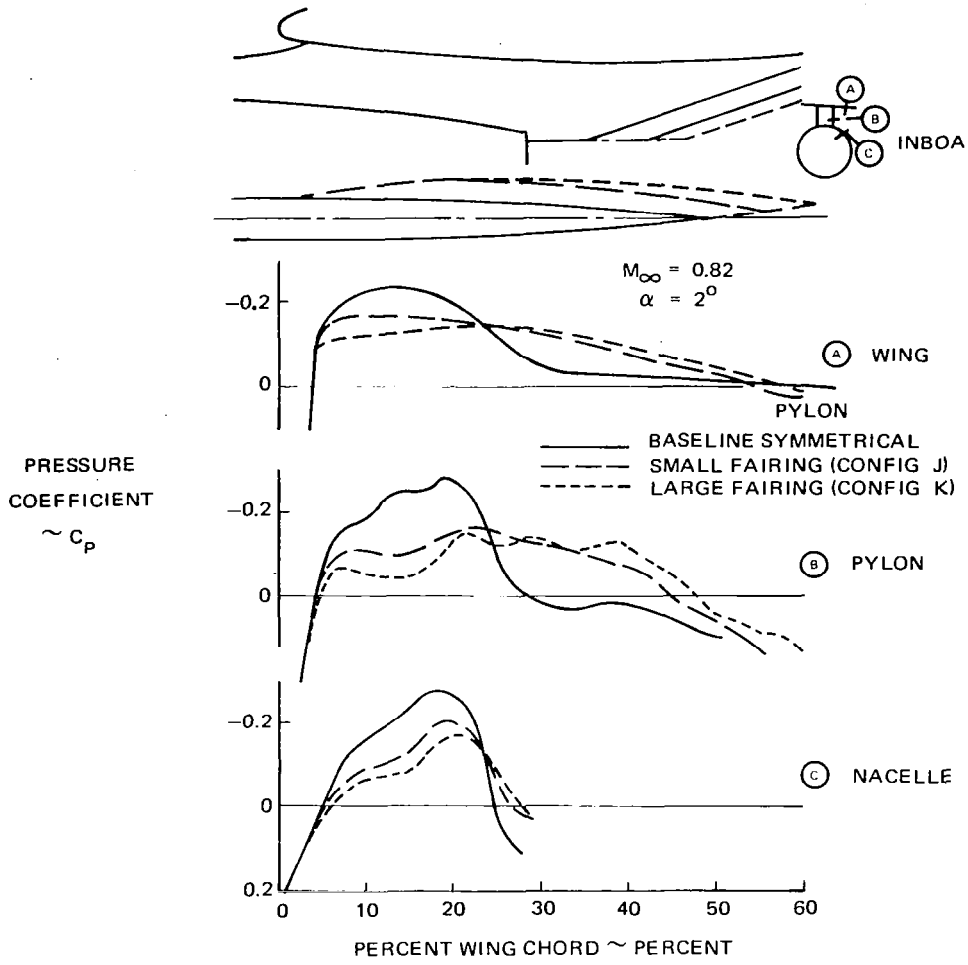

FIGURE 18. EFFECT OF PYLON FAIRINGS ON INBOARD CHANNEL PRESSURES

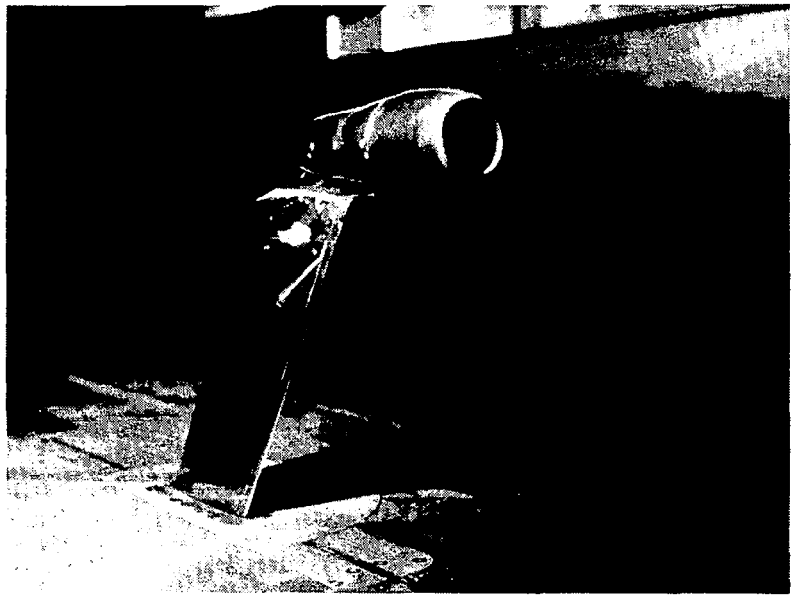

FIGURE 19. ISOLATED NACELLE MODEL INSTALLATION

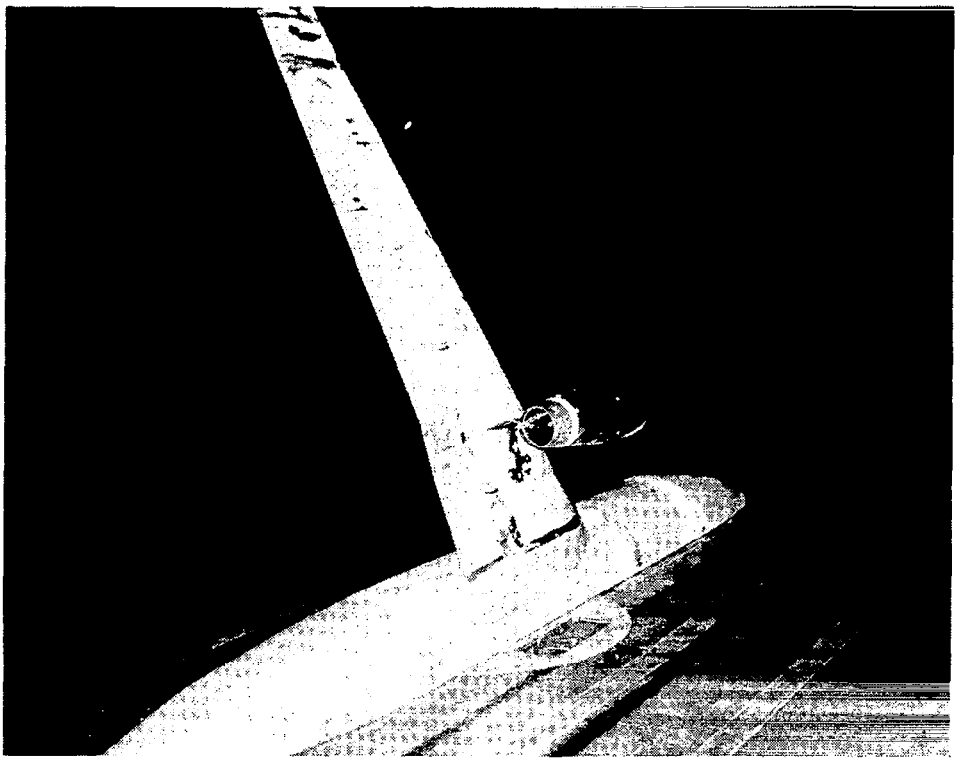

FIGURE 20. SEMISPAN MODEL INSTALLATION

engine jet. The external lines of the flow-through LDN were also designed for the CF6-50 engine. The powered LDN having a coplanar exit contained a TD-460 turbosimulator. The nacelle model geometries are shown in Figure 21.

The nacelles and pylons were instrumented with a row of static pressure orifices on the inboard sides.

Test Conditions and Measurements — Measurements were taken over a Mach number range of 0.60 to 0.84. Isolated nacelle measurements were taken with the nacelle installed at zero angle of attack. A Reynolds number of 22.96 x 10^6 per meter (7.0 x 10^6 per foot) was held constant for these measurements. For the semispan test, the angle of attack was varied from 1 degree to 4 degrees, corresponding to lift coefficient values between 0.30 to 0.60. A Reynolds number of 18.0 x 10^6 per meter (5.5 x 10^6 per foot) was held constant for the semispan model tests. The turbosimulator was set to nozzle pressure ratios representative of cruise conditions.

A five-component external balance was used to obtain the force and moment data. Side force measurements were not taken. The angle of attack was measured with a Douglas-furnished system which utilizes two linear potentiometers. Static pressures were measured during the semispan test. Chordwise pressure distributions on the wing were measured on the top and bottom surfaces. Additional information on the flow condition was provided by photographs

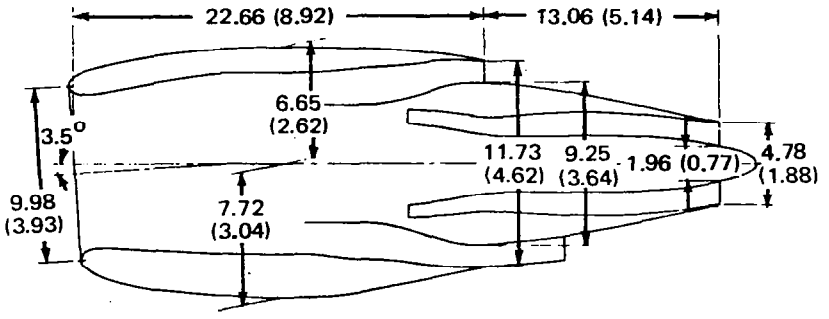

POWERED SDN

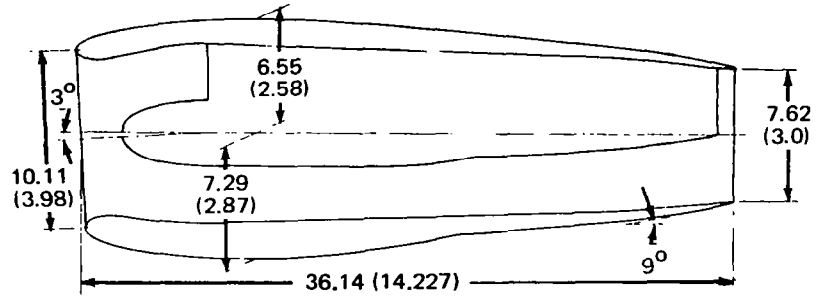

FLOW-THROUGH LDN

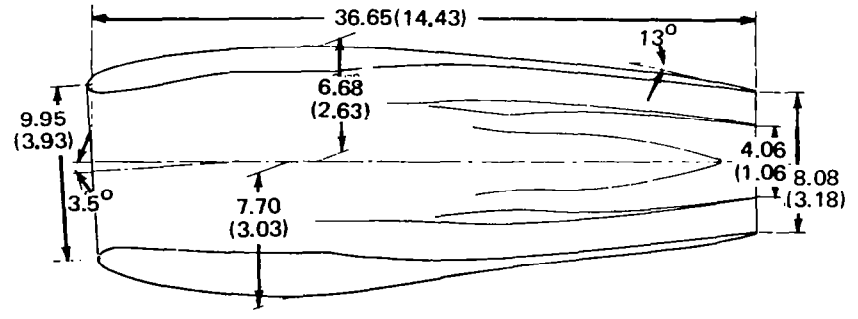

POWERED LDN

DIMENSIONS ARE IN CENTIMETERS (INCHES)

FIGURE 21. GEOMETRY OF NACELLE MODELS

of fluorescent minitufts located on the inboard sides of the nacelles and pylons. For the powered model, additional measurements taken were inlet static pressures, and fan and turbine duct rake total and static pressures. Turbosimulator measurements consisted of fan and turbine duct air temperature, drive air pressures, and engine revolutions per minute.

Test Procedure — The procedure for determining the interference drag of the nacelle installations was as follows:

- The isolated nacelle plus pylon drag was determined as the difference between the drag of nacelle, pylon, and strut minus the strut tare.
- The drag of the wing/body was measured.
- The drag of the complete semispan model was measured.
- The excess installation drag (interference drag) was the difference between the complete semispan model drag coefficient and the sum of the drag coefficients of the wing/body, isolated nacelle, and pylon compared at constant lift coefficient.

The isolated nacelle and pylon conbination was calibrated at zero angle of attack. The isolated data were not corrected for the internal drag of the nacelle.

Accuracy of Data — Reynolds number was held to within ±328,000 per meter (±100,000 per foot) and Mach number to within ±0.002 of the specified value. Data for the wing/body and with the flow-through LDN were quite repeatable with little scatter. During the testing, a small but significant malfunction of the angle-of-attack system was discovered. A correction was devised and successfully applied to the data. The repeatability of the data was such that the conclusions of the report would be unaffected by the lack of these small corrections.

The quality of the powered nacelle test data was much poorer than that of the flow-through data. Absolute drag levels shifted, and significant differences in interference drag appeared at 0.6 Mach number. At this Mach number, all configurations should be free of interference effects, and therefore interference drag should be zero. The problem is probably related to the calculation of simulator thrust, which required calibration data utilizing internal pressure measurements. It was not possible to determine engine thrust directly because of contamination of the turbosimulator internal pressure instrumentation by oil leakage. Furthermore, an alternative approach measuring engine revolutions per minute did not yield satisfactory results.

It was determined that the powered force data were irretrievable and that conclusions should not be drawn from them. Therefore, the conclusions relating to powered forces are based on the flow-through nacelle force data. Wing-pylon-nacelle channel pressure data were used to assess the power effects on the LDN installation.

Results and Discussion

Summary results are presented at Mach numbers and lift coefficients typical of cruise conditions for the aircraft, namely Mach number of 0.82 and C_L of 0.50.

The measured drag coefficient (including internal drag) of the isolated flow-through LDN and symmetrical pylon was nearly a constant C_D = 0.002 (20 counts) and was independent of the Mach number.

Semispan Flow-Through LDN — The interference drag for the flow-through LDN with the baseline pylon is shown in Figure 22.

At the cruise condition (M_∞ = 0.82 and C_L = 0.50), the aircraft interference drag coefficient is about 0.00015 (approximately 0.5 percent of airplane drag) and does not show significant Mach number dependency. Inboard channel pressures from the test are shown in Figure 23. Flow in the channel became critical at about M_∞ = 0.80, resulting in peak Mach numbers across the channel of about 1.1 at a Mach number of 0.82. This peak is well below the M = 1.3 to 1.4 levels which have been known to cause nacelle afterbody flow separation with an attendant drag problem for similar type installations.

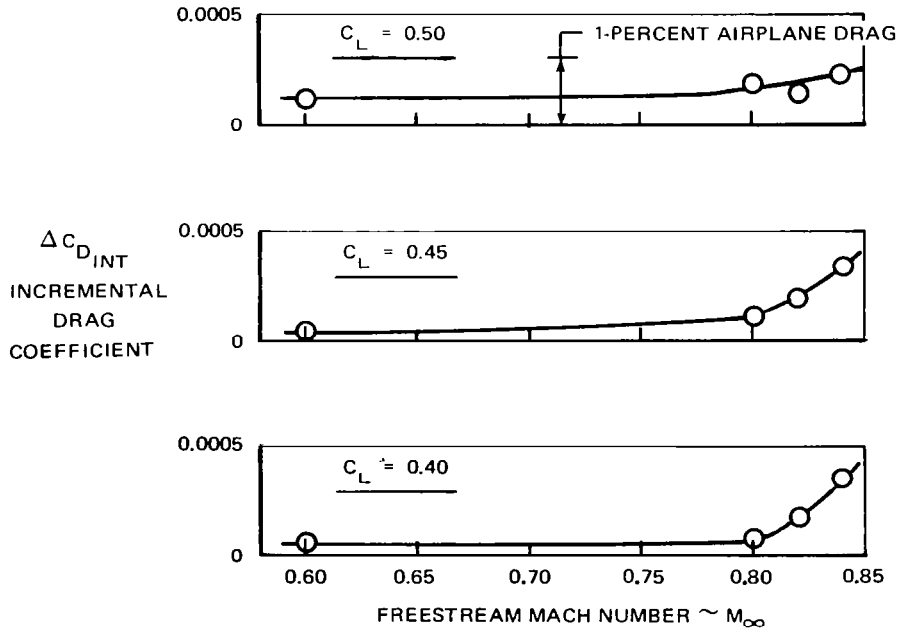

FIGURE 22. INTERFERENCE DRAG CHARACTERISTICS FOR FLOW-THROUGH LDN WITH BASELINE PYLON

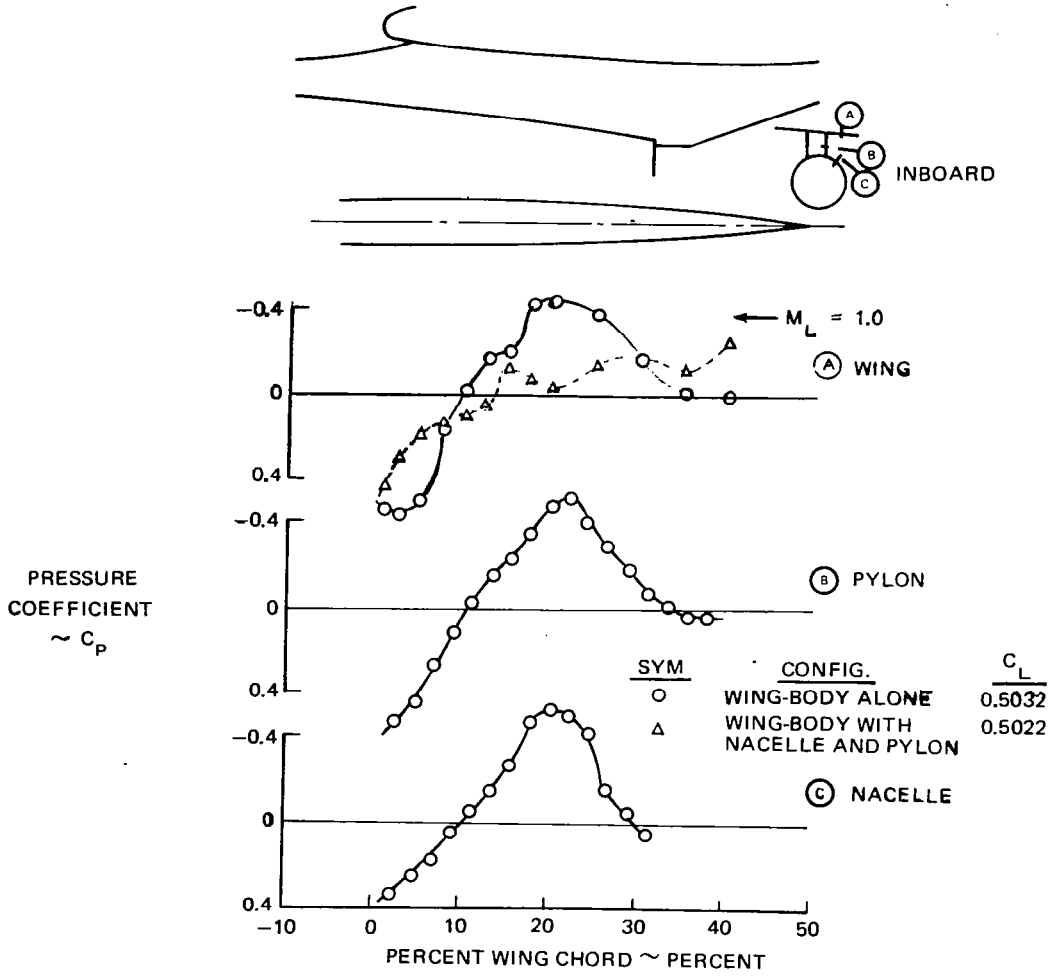

FIGURE 23. EFFECT OF FLOW-THROUGH LDN ON CHANNEL PRESSURES – BASELINE PYLON

Tuft observations on the LDN afterbody and pylon show complete flow attachment. To further evaluate these data, a boundary layer analysis was undertaken using measured pressure distribution. This analysis included scrutiny of results on the SDN tests, in which peak suction pressures did not show quite the criticality measured in previous wind tunnel tests and flight tests. The analysis, when corrected to account for these differences, revealed no tendency toward flow separation on the nacelle afterbody at test conditions or flight conditions.

Powered LDN – A comparison of inboard channel pressures for the flow-through and powered LDN installations is shown in Figure 24. No effect of LDN power simulation on these pressures was detected. It is concluded, therefore, that power effects do not change the channel flow mechanism. This also implies that the flow-through LDN force results are directly applicable, because the interference mechanisms are not power-dependent.

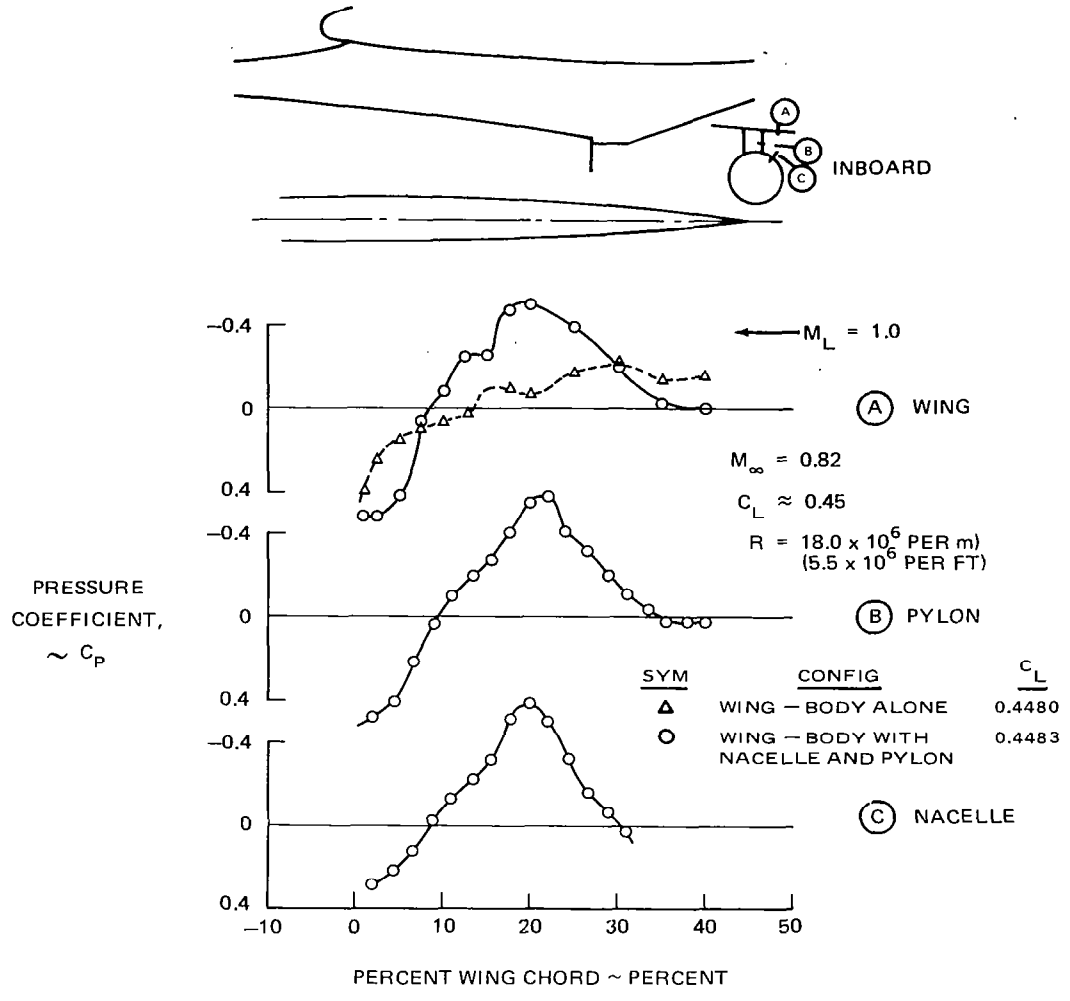

FIGURE 24. EFFECT OF LDN INSTALLATION ON INBOARD CHANNEL PRESSURES – BASELINE SYMMETRICAL PYLON (M_∞ = 0.82, C_L = 0.45)

Nacelle Incidence Angle — The test results showed that the incidence of the current installation is optimum for the LDN. Incidence angle changes lesser or greater than the current DC-10 SDN configuration resulted in a drag increase (Figure 25). Wing-pylon-nacelle channel pressures indicated that the channel was slightly less critical with an increase or decrease in incidence angle, suggesting that the drag penalty was entirely due to nacelle-induced drag. Measured incidence penalties were close to predictions made from isolated nacelle induced drag measurements, therefore reinforcing the conclusion that the channel peak velocities were not high enough to be of concern for the baseline symmetrical pylon.

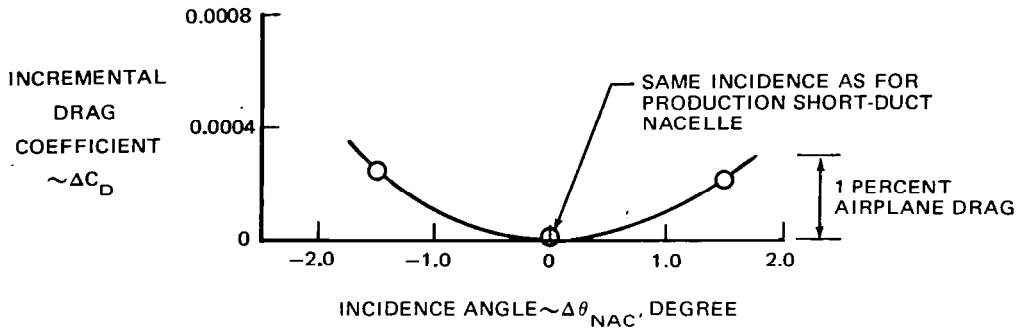

FIGURE 25. EFFECT OF NACELLE INCIDENCE ANGLE CHANGE ON INCREMENTAL DRAG

Pylon Fairing — Drag increments for Configuration J, the small pylon fairing (Figure 26), were about one-half of those for the baseline pylon at $C_L = 0.50$. The measuring system contains tolerances which may cast doubt on the negative drag increments at the lower lift coefficients at the lower Mach numbers. The peak pressure coefficients were reduced about $\Delta C_p = 0.1$ (Figure 27). Pressure gradients aft of the suction peaks were reduced appreciably on the wing and pylon, and slightly on the nacelle afterbody.

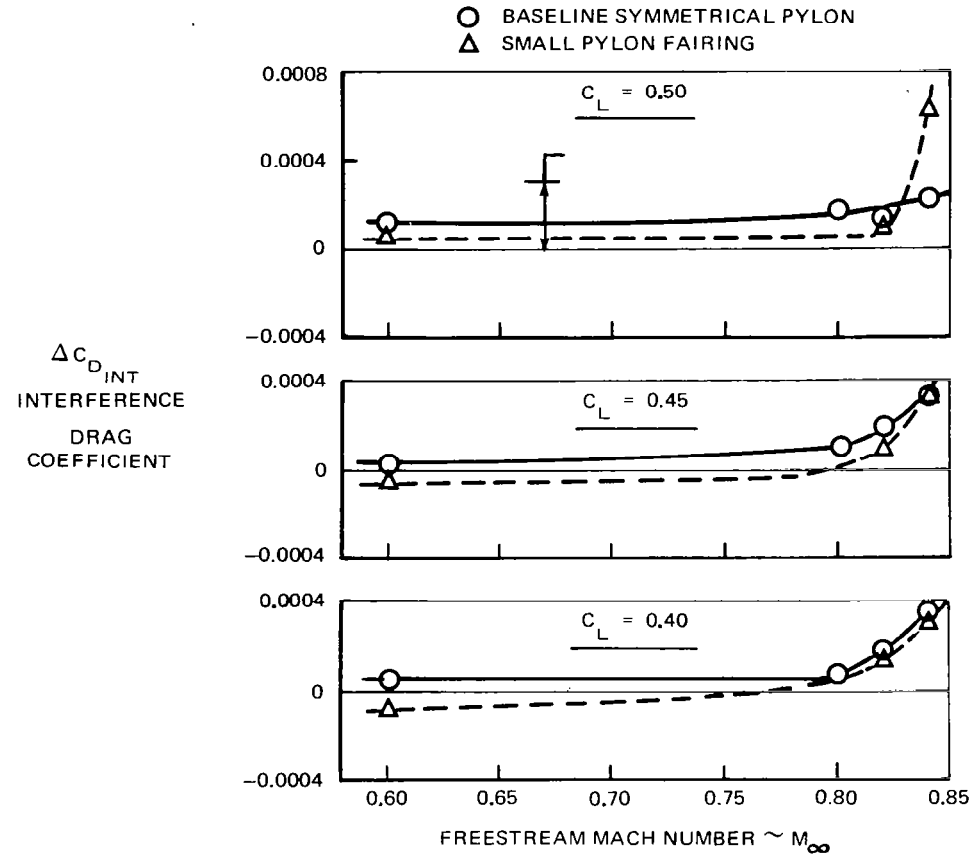

FIGURE 26. EFFECT OF SMALL PYLON FAIRING ON INTERFERENCE DRAG

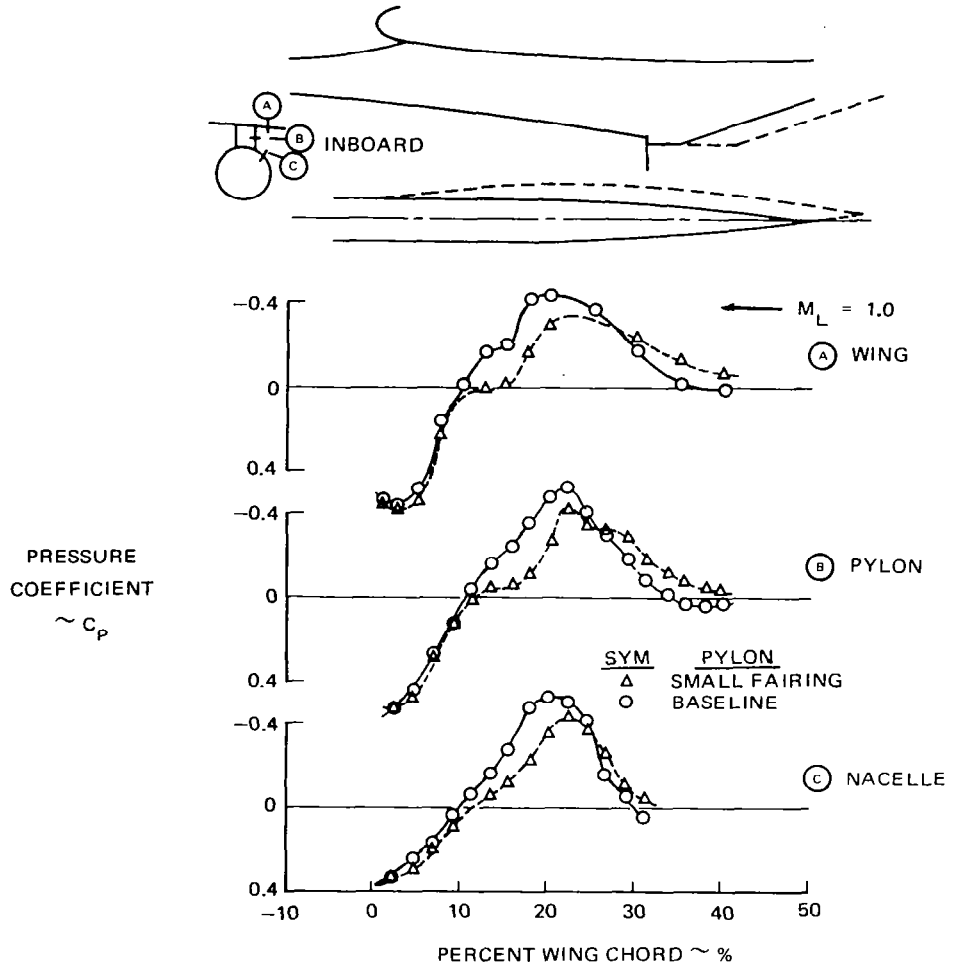

FIGURE 27. EFFECT OF SMALL PYLON FAIRING ON CHANNEL PRESSURES

Force data for Configuration K, the large pylon fairing, showed a higher drag level at 0.6 Mach number. The interference drag at 0.82 Mach number was about the same as the baseline. The inferiority of the large pylon fairing appears to be due to a lack of recovery on the nacelle afterbody and could even be the result of local flow separation. It may be possible that a fairing derived from either of those tested may offer an improvement in performance relative to the small pylon fairing.

CONCLUSIONS

Winglet

Winglets on the DC-10 provided approximately twice the cruise drag reduction of wing-tip extensions with approximately the same increase in bending moment at the wing-fuselage juncture. Furthermore, the winglet configurations achieved drag reductions which were in close agreement with analytical estimates. The wing-tip extension achieved the full analytical drag reduction potential. Relatively small changes in wing-winglet tailoring effected large improvements in drag and flow characteristics. Careful longitudinal spacing of the upper and lower surface weights proved significant in preventing adverse compressibility effects. All final winglet configurations exhibited good visual flow characteristics on the wing and winglets.

Long-Duct Nacelle

The LDN with the current production nacelle had a low interference drag of 0.5-percent aircraft drag or less, relative to an interference free installation. In addition, the alternative pylon with a small aft fairing reduced channel pressure, which resulted in a reduction of the interface drag to an insignificant level. A larger fairing was not as effective. The optimum LDN incidence was the same as that of the current nacelle, thus enabling the current engine mounting primary structure to be retained. Wing-pylon-nacelle channel pressure distributions were not essentially different with powered simulation on flow-through nacelles. This indicates that the channel flow was not affected by the exhaust pressure ratio; hence, power effects are considered to be negligible.

TECHNOLOGY RECOMMENDATIONS

Winglet

For the immediate future the following technology is recommended in association with the EET project:

- Aerodynamic development in the high-lift mode
- Definition of the aerodynamic stability and control characteristics
- Investigation of the flutter characteristics
- Assessment of the installation impact due to the findings of the EET work and relevant Douglas studies on key mission performance factors.

This work has been authorized under Contract NAS1-15327 (EET Phase II). In order to expedite the activity and employ the available test facilities, the preparation of plans, designs, and long-lead test models has been authorized under the present contract.

Continuation of this work should focus on the structural application of winglets and particularly on the extension of technology to minimize any penalty of incorporation. Particularly appropriate is the work related to active controls (wing load alleivation and flutter suppression) which is influenced by the interaction of the winglet and outboard aileron.

The degree of success in this work will point the way to production application or further recommendations. At this time, the concept of a flight demonstration prior to production commitment must also be entertained.

The rationale and approach for these recommendations are given below.

High-Lift Aerodynamics – Available experimental data on the characteristics of a wing/winglet combination in the high-lift configuration are for wings operating at substantially lower maximum lift coefficient than those of the DC-10. The winglet is likely to operate at a higher normal force coefficient than the wing's lift coefficient. With the expected performance requirement, a risk exists that winglet separation may occur, leading to loss of wing lift. The extent of the performance requirement for the winglet is shown in Figure 28. The data result from an analysis of the DC-10, including fuselage and winglets, using the Douglas Nonplanar Lifting Systems Program. The analysis accounted for wing flap and slat effects at cruise, takeoff, and landing positions, and established the winglet section life coefficients as a function of aircraft lift coefficient. From this assessment, it was determined that the high-lift behavior of the wing and winglet should be investigated to the extent that a requirement for a winglet leading-edge device to delay separation should be explored. A slat concept was preferred. Design criteria for the device are summarized in Figure 29. A slat design was prepared using these criteria and previous experience. Its performance was evaluated using the Douglas Neumann Potential Flow Program. A low-speed test is planned for the NASA Ames 12-foot facility. The basic model is an existing

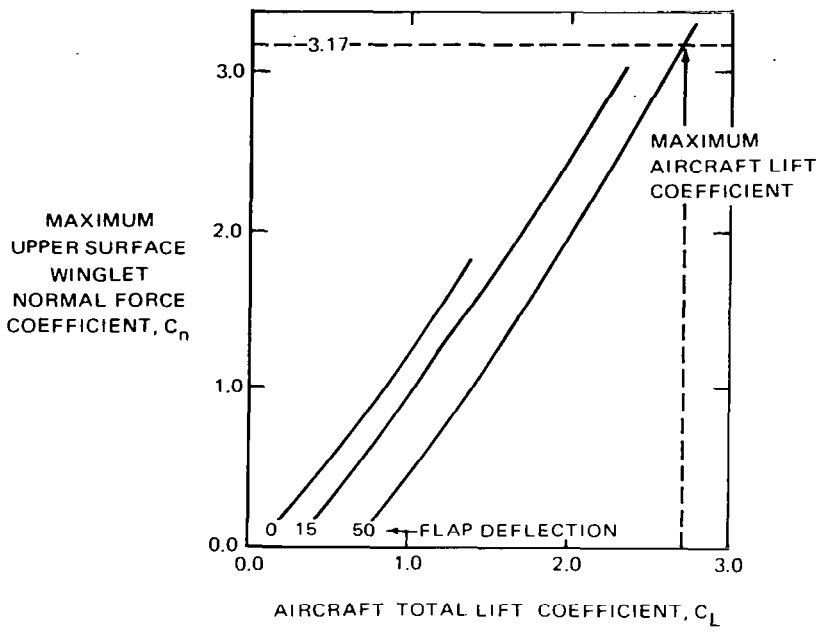

FIGURE 28. MAXIMUM WINGLET NORMAL FORCE COEFFICIENT

EMPLOY PRELIMINARY STRUCTURAL GUIDELINES, SINCE A DETAILED WINGLET STRUCTURAL DESIGN IS NOT AVAILABLE

- SLAT TRAILING EDGE POINT AT 15-PERCENT CHORD
- WING UNDERSLAT SURFACE (WUSS) TANGENCY POINT ONE PERCENT AFT OF SLAT TRAILING EDGE
- SLAT-TRAILING-EDGE ANGLE EQUAL TO 6 DEGREES

LIMIT MINIMUM PRESSURE COEFFICIENTS TO VALUES CONSISTENT WITH 9-PERCENT TWO-DIMENSIONAL SUPERCRITICAL AIRFOIL TEST RESULTS

- MINIMUM SLAT-PRESSURE COEFFICIENT EQUAL TO -12
- MINIMUM (WUSS)-PRESSURE COEFFICIENT EQUAL TO -8

FIGURE 29. UPPER WINGLET SLAT DESIGN CRITERIA

Douglas-furnished 4.7-percent-scale full-span DC-10-30. The test will also establish stability and control characteristics.

High-Speed Aerodynamics – The effects of the winglet concept of the aerodynamic characteristics will be evaluated by a wind tunnel test planned for the NASA Ames 11-foot facility, with the basic model being an existing Douglas-furnished 3.25-percent-scale full-span DC-10-30. The results of this test will expand the data base which is limited for second-generation transport aircraft such as the DC-10.

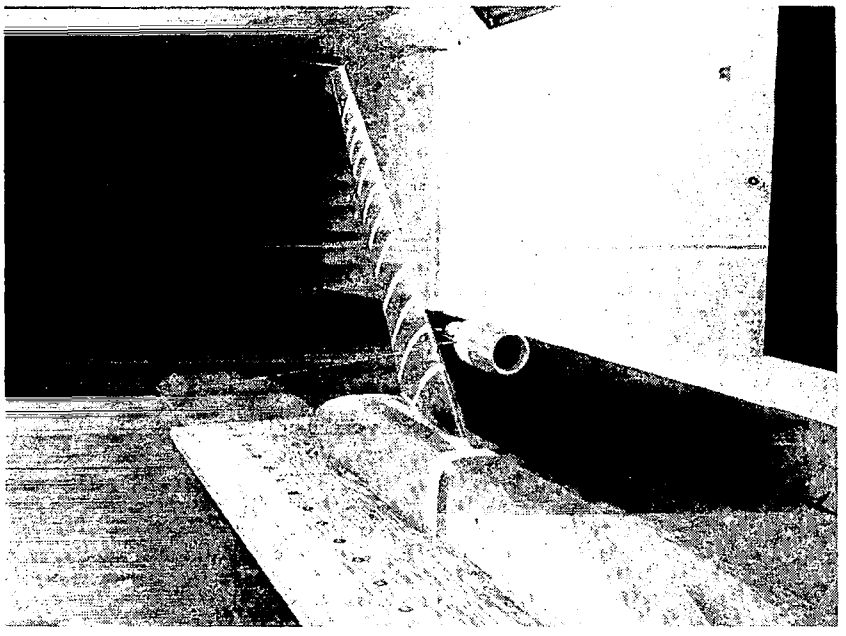

FIGURE 30. SEMISPAN WINGLET FLUTTER MODEL

Flutter Investigation — Analyses of winglet installations commonly predict an adverse effect on the flutter speed of an aircraft, and this prediction is confirmed by preliminary work for the DC-10. There is some concern that the true effect of a winglet may be even greater than that suggested by the analysis, particularly with transonic flow conditions. While it would be desirable to conduct a comprehensive flutter program encompassing subsonic and transonic tests, it is intended initially to investigate subsonic behavior only, using a semispan model. This program will conduct analyses and tests on an existing subsonic DC-10 wing flutter model fitted with winglets. The subsonic testing is planned for the Northrop 7- by 10-foot subsonic wind tunnel, the basic model being an existing Douglas-furnished 4.5-percent-scale semispan DC-10-30. The model with winglets is shown in Figure 30.

Installation Effects — It is proposed that the findings of the aerodynamic and flutter investigations and of previous work done at Douglas on the structural installation be evaluated to present the combined effects. This evaluation will present the impact in terms of weight and other significant performance parameters such as mission range.

Active Control Technology — As a continuation of the work described above, it is proposed that further activity focus on maximizing the net performance gain of the winglet installation.

With regard to the current rapid progress in the technology, it is appropriate to consider the application of active controls to the winglet application. The following activity should be considered:

- Semispan wing/aileron wind tunnel tests at low speed and high speed. These will investigate the behavior of the aileron in the presence of the winglet so as to determine its use in wing load alleviation of the winglet.
- Transonic flutter test and analysis, to determine the aerodynamic effects on wing flutter.
- Winglet active control flutter test and analysis, semispan and full span, to determine gust load alleviation and flutter characteristics and flutter suppression behavior.
- Wing load alleviation and flutter suppression analysis and design.
- Investigation of the design requirements of an actuator development from DC-10 to cover flutter suppression.
- Extended integration analysis to determine the impact of all the above on the DC-10 principal performance characteristics.

Long-Duct Nacelle

The originally proposed program for the LDN concept development included a Douglas-funded mixer model test to identify the internal nacelle flow benefits, an EET wind tunnel test to minimize the external propulsion-airframe interference, and a joint Douglas/EET DC-10 flight test to demonstrate the design. As a result of the aerodynamic interference model test work, it is now no longer regarded necessary to verify the propulsion-airframe interference in flight.

Promising results have been obtained in the mixer model test. However, one finding was that additional mixing length was needed in the nacelle. The investigation of the impact of this result on the aerodynamic interference is recommended for further wind tunnel tests.

Since it is believed that confidence on the aerodynamic interference can be provided with the wind tunnel test conclusions, uncertainty in preparing an eventual performance guarantee becomes linked with demonstration of internal performance, which is the responsibility of the engine manufacturer. It has not been proven possible to obtain engineering manufacturers' commitments to such a guarantee within the time and resource budgets of EET. It has been concluded that these resources would be better channeled into an airframe-related activity, such as winglets.

The rationale and approach for the recommended work under EET is discussed below. To further advance the definition of high-speed characteristics, a test in the Calspan wind tunnel is planned. The test has three purposes. The first and primary purpose arises primarily from the finding in the mixer model tests that a somewhat different nacelle afterbody may be required to

attain satisfactory mixer performance. The requirement, to reduce internal duct Mach numbers into the mixer, effectively translates to a larger duct diameter at the mixer plane and a longer nozzle length. It therefore becomes necessary to identify the effect of this nacelle on the channel velocities.

A secondary purpose of the test is related to the differences in the measured channel velocities (see LDN results and discussion) test for the SDN compared to flight data, the flight data being more severe. This difference would probably also apply to the LDN. A suitable adjustment to the pressure data, however, did not appear to invalidate the general conclusion that the interference drag on the LDN was very small. Recently, channel pressures have been measured in flight on a short primary nacelle. In contrast to the Ames tests for this configuration, the channel pressures were lower than those measured on the model. In order to explore this inconsistency further, it is proposed to rerun the baseline LDN in the Calspan facility. In this facility, reasonably good correlation has previously been obtained with flight-measured channel data.

A third purpose is the measurement, within the capabilities of the facility, of the incremental drag of the new shape LDN compared with the baseline LDN.

REFERENCES

1. Gilkey, R. D.: Design and Wind Tunnel Tests of Winglets on a DC-10 Wing. NASA CR 3119, April 1979.

2. Patel, S. P.; and Donelsen, J. E.: Investigation of the Interference Effects of Mixed-Flow Long-Duct Nacelles on a DC-10 Wing. NASA CR 159202, March 1980.

3. Whitcomb, Richard T.: A Design Approach and Selected Wind Tunnel Results at High Subsonic Speeds for Wing-Tip Mounted Winglets. NASA TN D-8260, July 1976.

4. Nordstrom, K. E.; March, A. H.; and Sargisson, D. F.: Conceptual Design Study of Advanced Acoustic Composite Nacelles. NASA CR 132703, July 1975.

1. Report No.	2. Government Accession No.	3. Recipient's Catalog No.
NASA CR-3296		

4. Title and Subtitle	5. Report Date
SELECTED WINGLET AND MIXED-FLOW LONG-DUCT NACELLE DEVELOPMENT FOR DC-10 DERIVATIVE AIRCRAFT - SUMMARY REPORT	June 1980
	6. Performing Organization Code

7. Author(s)	8. Performing Organization Report No.
A. B. Taylor	ACEE-05-FR-9912
	10. Work Unit No.

9. Performing Organization Name and Address	11. Contract or Grant No.
Douglas Aircraft Company McDonnell Douglas Corporation 3855 Lakewood Boulevard Long Beach, California 90846	NAS1-14743
	13. Type of Report and Period Covered

12. Sponsoring Agency Name and Address	13. Type of Report and Period Covered
National Aeronautics and Space Administration Washington, D.C. 20546	Contractor Report
	14. Sponsoring Agency Code

15. Supplementary Notes

Langley Technical Monitor: Donald L. Maiden
Final Report

16. Abstract

Activities to investigate the high-speed cruise drag effects of the installation of winglets and a wing-tip extension and of a mixed-flow long-duct nacelle are summarized. The winglet program utilized a 4.7-percent semispan model in the Langley Research Center 8-foot transonic wind tunnel. Winglets were found to provide approximately twice the cruise drag reduction of wing-tip extensions for about the same increase in bending moment at the wing-fuselage juncture. The long-duct nacelle interference drag program utilized the same model, without the winglets, in the Ames Research Center 11-foot transonic wind tunnel. The long-duct nacelle, installed in the same position as the current short-duct nacelle and with the current production symmetric pylon, was found to be a relatively low-risk installation. A pylon with an additional small rearward fairing was also tested and showed some drag reduction potential over the current pylon. The report includes technology recommendations for follow-on work: for the winglet, aerodynamic wind tunnel testing, identification of flutter characteristics, and integration study; and for the long-duct nacelle, aerodynamic wind tunnel testing to evaluate nacelle shape changes.

17. Key Words (Suggested by Author(s))	18. Distribution Statement
Winglets Cruise drag reduction Long-duct nacelle	FEDD Distribution Subject Category 05

19. Security Classif. (of this report)	20. Security Classif. (of this page)	21. No. of Pages	22. Price
Unclassified	Unclassified	47	

Available: NASA's Industrial Application Centers

NASA-Langley, 1980